

AD-A111 208

NAVAL POSTGRADUATE SCHOOL MONTEREY CA

F/G 11/6

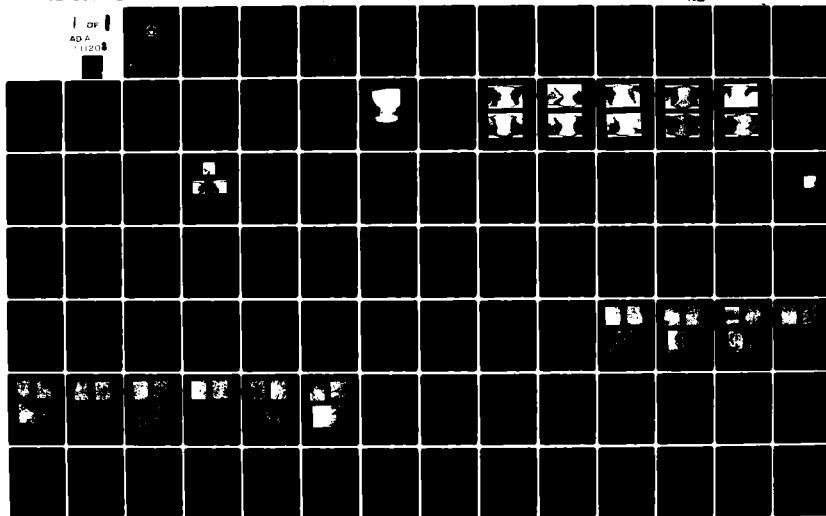
A CORRELATION BETWEEN THE HEAT AFFECTED ZONE MICROSTRUCTURE AND—ETC(U)
 SEP 81 M J SOREK

SEP 81 M J SOREK

UNCLASSIFIED

NL

1 of 1
AD A
1110



AD A111208

DTIC FILE COPY

2

NAVAL POSTGRADUATE SCHOOL

Monterey, California



DTIC
FILE COPY
B

THESIS

A CORRELATION BETWEEN THE HEAT
AFFECTED ZONE MICROSTRUCTURE AND THE
THERMAL HISTORY DURING WELDING OF HY-130 STEEL

by

Michael Joseph Sorek

September 1981

Thesis Advisor:

K.D. Challenger

Approved for public release; distribution unlimited.

REPORT DOCUMENTATION PAGE		READ INSTRUCTIONS BEFORE COMPLETING FORM
1. REPORT NUMBER	2. GOVT ACCESSION NO.	3. RECIPIENT'S CATALOG NUMBER
	AD-A111 208	
4. TITLE (and Subtitle) A Correlation Between the Heat Affected Zone Microstructure and the Thermal History During Welding of HY-130 Steel		5. TYPE OF REPORT & PERIOD COVERED Master's Thesis September 1981
		6. PERFORMING ORG. REPORT NUMBER
7. AUTHOR(s) Michael Joseph Sorek		8. CONTRACT OR GRANT NUMBER(s)
9. PERFORMING ORGANIZATION NAME AND ADDRESS Naval Postgraduate School Monterey, California 93940		10. PROGRAM ELEMENT PROJECT TASK AREA & WORK UNIT NUMBERS
11. CONTROLLING OFFICE NAME AND ADDRESS Naval Postgraduate School Monterey, California 93940		12. REPORT DATE September 1981
		13. NUMBER OF PAGES 95
14. MONITORING AGENCY NAME & ADDRESS (if different from Controlling Office)		15. SECURITY CLASS. (of this report)
		15a. DECLASSIFICATION/DOWNGRADING SCHEDULE
16. DISTRIBUTION STATEMENT (of this Report) Approved for public release; distribution unlimited.		
17. DISTRIBUTION STATEMENT (of the abstract entered in Block 20, if different from Report)		
18. SUPPLEMENTARY NOTES		
19. KEY WORDS (Continue on reverse side if necessary and identify by block number) HY-130 Steel Weldments Welding Thermal History Heat Affected Zone Microstructure in HY-130 Steel		
20. ABSTRACT (Continue on reverse side if necessary and identify by block number) → A study of microstructure as a function of distance from the fusion line was conducted for an instrumented weld in HY-130 steel plate. Thermocouples were positioned in the plate at various distances from the fusion line and were used to obtain the welding thermal history at these locations. A correlation was then developed between the microstructures observed and the thermal history experienced. Additionally,		

the tempering of the heat affected zones of the initial weld passes by subsequent weld passes was calculated and correlated with hardness and microstructural data. Finally, a further study of the "metallurgical notch" phenomenon postulated by Brucker was undertaken.

Accession For

NTIS GRA&I

DTIC TAB

Unannounced

Justification

By

Date of Report

Availability Codes

Avail and/or

Distribution

A

Approved for public release; distribution *UNLIMITED*

A Correlation Between the Heat Affected
Zone Microstructure and the Thermal History During
Welding of HY-130 Steel

by

Michael Joseph Sorek
Lieutenant Commander, United States Navy
B.S. Eng., Purdue University, 1973

Submitted in partial fulfillment of
the requirements for the degree of

MASTER OF SCIENCE IN MECHANICAL ENGINEERING

from the

NAVAL POSTGRADUATE SCHOOL
September 1981

Author:

Michael J. Sorek

Approved by:

Kenneth D. Challenor

Thesis Advisor

Larry R. McNelly

Second Reader

J. J. Marto

Chairman, Department of Mechanical Engineering

William M. Tolles

Dean of Science and Engineering

ABSTRACT

A study of microstructure as a function of distance from the fusion line was conducted for an instrumented weld in HY-130 steel plate. Thermocouples were positioned in the plate at various distances from the fusion line and were used to obtain the welding thermal history at these locations. A correlation was then developed between the microstructures observed and the thermal history experienced. Additionally, the tempering of the heat affected zones of the initial weld passes by subsequent weld passes was calculated and correlated with hardness and microstructural data. Finally, a further study of the "metallurgical notch" phenomenon postulated by Brucker was undertaken.

TABLE OF CONTENTS

I.	INTRODUCTION AND BACKGROUND-----	11
A.	PREVIOUS RESEARCH EFFORTS-----	11
B.	THE INSTRUMENTED WELD-----	12
C.	SCOPE AND OBJECTIVES OF CURRENT RESEARCH-----	14
II.	EXPERIMENTAL PROCEDURE-----	16
A.	MACRO SAMPLES-----	16
1.	Preparation-----	16
2.	Physical Measurements-----	19
B.	METALLOGRAPHIC SAMPLES-----	19
C.	HARDNESS MEASUREMENTS-----	25
D.	ANALYSIS OF TIME-TEMPERATURE PLOTS-----	27
E.	CALCULATION OF THE TEMPERING PARAMETER-----	30
F.	CARBON EXTRACTION REPLICAS-----	36
III.	RESULTS AND DISCUSSION-----	37
A.	MACROSCOPIC EXAMINATION-----	37
B.	ROCKWELL HARDNESS MEASUREMENTS-----	40
C.	MICROHARDNESS MEASUREMENTS-----	40
D.	THERMAL HISTORY ANALYSIS-----	54
E.	MICROSTRUCTURAL ANALYSIS-----	56
1.	Thermocouple Locations 1-4, 3-4-----	57
2.	Thermocouple Locations 1-3, 3-3-----	57
3.	Thermocouple Locations 3-2, 1-2, 2-2-----	58
4.	Thermocouple Locations 1-1, 2-1, 4-1-----	60

F. ADDITIONAL OBSERVATIONS-----	63
IV. CONCLUSIONS-----	76
V. RECOMMENDATIONS-----	77
APPENDIX A MARE ISLAND NAVAL SHIPYARD WELDING PROCEDURE QUALIFICATION RECORD-----	78
APPENDIX B THERMAL HISTORY DATA OBTAINED FROM TIME TEMPERATURE PLOTS-----	83
LIST OF REFERENCES-----	93
INITIAL DISTRIBUTION LIST-----	95

LIST OF TABLES

I.	Identification, Chemical Composition and Heat Treatment Data for Test HY-130 Plate-----	13
II.	Physical Data for Selected Thermocouple Locations-----	38
III.	Rockwell Hardness Data, Temper Bead Sequence-----	41
IV.	Rockwell Hardness Data, Root of the Weld-----	42
V.	Rockwell Hardness Data, Straight Bead Sequence-----	43
VI.	Microhardness Data for Thermocouple Attachment Points-----	53

LIST OF FIGURES

1.	Macro Sample of Welded Plate Showing Thermocouple Placement-----	17
2.	Example of Resolution of Weld Area Possible with Ammonium Persulphate Etch-----	18
3.	Location of Thermocouple 1-1-----	20
4.	Location of Thermocouple 1-2-----	20
5.	Location of Thermocouple 1-3-----	21
6.	Location of Thermocouple 1-4-----	21
7.	Location of Thermocouple 2-1-----	22
8.	Location of Thermocouple 2-2-----	22
9.	Location of Thermocouple 3-2-----	23
10.	Location of Thermocouple 3-3-----	23
11.	Location of Thermocouple 3-4-----	24
12.	Location of Thermocouple 4-1-----	24
13.	Diagram of Rockwell Hardness Traverse Locations-----	26
14.	Diagram of Micro Specimen Cutting Locations-----	28
15.	Locations of Microhardness Traverses-----	29
16.	Time-Temperature Plot for Thermocouple 2-1, Pass 12-----	31
17.	Time-Temperature Plot for Thermocouple 2-1, Passes 13, 14, 15-----	32
18.	Isothermal Transformation Diagram for HY-130 (T) Steel-----	35
19.	Peak Temperature vs. Distance From Fusion Line After Welding-----	39

20.	Microhardness Traverse Results for Location Indicated in Figure 15a-----	45
21.	Microhardness Traverse Results for Location Indicated in Figure 15c-----	46
22.	Microhardness Traverse Results for Location Indicated in Figure 15b(1)-----	48
23.	Microhardness Traverse Results for Location Indicated in Figure 15b(2)-----	49
24.	Location 1-4, 12.2 mm From the Fusion Line After Welding-----	64
25.	Location 3-4, 12.4 mm From the Fusion Line After Welding-----	65
26.	Location 1-3, 7.25 mm From the Fusion Line After Welding-----	66
27.	Location 3-3, 8.4 mm From the Fusion Line After Welding-----	67
28.	Location 3-2, 5.6 mm From the Fusion Line After Welding-----	68
29.	Location 1-2, 3.9 mm From the Fusion Line After Welding-----	69
30.	Location 2-2, 4.2 mm From the Fusion Line After Welding-----	70
31.	Location 1-1, at the Fusion Line After Welding-----	71
32.	Location 2-1, 1.0 mm From the Fusion Line After Welding-----	72
33.	Location 4-1, 0.4 mm From the Fusion Line After Welding-----	73

ACKNOWLEDGEMENTS

I wish to express my sincere appreciation to my thesis advisor, Professor Ken Challenger, for his guidance in this research effort. I would also like to thank Professor Terry McNelley for his advice and comments, Professor Mike Edwards for stimulating my interest in Materials Science and Metallurgy, and Mr. Tom Kellogg for his assistance in the laboratory.

Special thanks is extended to my wife, Eddy, for her patience and understanding during these past two years, and to Ms. Carol Alejo for undertaking the typing of this document from a handwritten copy.

I. INTRODUCTION AND BACKGROUND

A. PREVIOUS RESEARCH EFFORTS

Over a period of approximately ten years a considerable research effort has been mounted to produce a successful replacement for HY-80 steel for submarine hull applications. The projected follow-on, HY-130, is a 0.1% carbon alloy steel containing approximately 5% nickel and lesser amounts of several other alloying elements.

Previous studies have led to the drafting of the specifications for production of forged, wrought and cast HY-130 steel [Ref. 1,2,3]. Other research by Connor, et al [Ref. 4], Flax, et al [Ref. 5] and others have determined the optimum parameters for welding HY-130 steel for a variety of welding techniques. Several studies have been conducted at the Massachusetts Institute of Technology by Masubuchi [Ref. 6] and others under contract to the Office of Naval Research to determine the stresses induced during welding and the residual stresses that may remain after welding HY-130.

Studies by Rogalski [Ref. 7] and Mabry [Ref. 8] included test welds instrumented with thermocouples as well as strain gages. These test welds placed thermocouples no closer than 0.5 inches (12.7 mm) to the weld and were spaced at varying distances from the weld. Additionally, Lipsey [Ref. 9] used a computer program to predict the temperature at various

locations in the test plate. In all of these tests however, no effort was made to measure or predict the temperature during welding closer than 0.5 inches (12.7 mm) to the fusion line.

Recent investigations into the catastrophic failure during explosion bulge testing of a cast HY-130 plate pointed out the need to further investigate the effects of the welding process on the metal surrounding the welded area of the plate. The explosion bulge test (EBT) is described by Brucker [Ref. 10] and detailed in a Department of the Navy Specification [Ref. 11]. Brucker reported that cracks produced in test plates which had undergone the EBT initiated and propagated through the heat affected zone (HAZ) of the plates. His investigation led to the postulation that a "metallurgical notch" had been created in the HAZ by the welding process and that this was a contributing factor in the catastrophic failure of one of the plates.

B. THE INSTRUMENTED WELD

The decision was made to perform an instrumented weld using the plate dimensions of the explosion bulge test sample in an effort to better characterize the welding process and the metallurgical consequences resulting from it. Two pieces of wrought HY-130 plate were provided by NAVSEA from their inventory at the Mare Island Naval Shipyard (MINSY). Each piece was 1 15/16 inches (4.92 cm) thick and measured 15 inches (38.1 cm) by 40 inches (101.6 cm). The chemical composition and heat treatment data for the test plates is presented in Table I.

TABLE I

Identification, Chemical Composition
and Heat Treatment Data for Test HY-130 Plate

Manufacturer: U.S. Steel Corporation
Heat No.: 5P4184
Plate No.: 050310
Thickness: 1 15/16 inches

Chemical Composition

<u>Element</u>	<u>Weight Percent</u>
Carbon	0.09
Manganese	0.78
Phosphorus	0.005
Sulfur	0.007
Silicon	0.29
Nickel	4.80
Chromium	0.55
Molybdenum	0.54
Vanadium	0.06
Titanium	0.004
Copper	0.08
Iron	Remainder

Heat Treatment

Austenitized at 1525°F for 3 hours, water quench.

Tempered at 1145°F for 3 hours, water quench.

Plate preparation and gas metal arc welding were conducted at MINSY according to specifications drawn by Brucker. (A complete description of the preparation and instrumentation appears in Reference 11.) The Welding Procedure Qualification Record from MINSY and diagrams of the thermocouple mounting arrangement are presented as Appendix A. It should be noted that the heat input during welding was maintained at 52,000 Joules per inch which was within the range of values recommended by Connor, et al [Ref. 12].

The temperature excursions experienced by the thermocouples were recorded on a Honeywell Model 5600E Analog Magnetic Tape Recorder. The tape was transferred to the Naval Postgraduate School (NPS) where time-temperature plots for each weld pass for each thermocouple were produced on a Gould Model 110 Strip Chart Recorder. The welded plate was also returned to NPS for further analysis.

C. SCOPE AND OBJECTIVES OF CURRENT RESEARCH

The present research effort was confined to a study of the microstructure of the metal from the instrumented weld plate using standard metallographic techniques.

Optical microscopy was used to determine the microstructure present and carbon extraction replicas were made for examination in the Transmission Electron Microscope (TEM) to determine the morphology and distribution of carbide particles present.

A determination of the correlation between the micro-structure at the thermocouple locations and the thermal history of those locations was sought. Additionally, an effort was made to determine the magnitude of tempering, if any, that might have been produced in the initial weld passes and their associated HAZ's by subsequent weld passes. Finally, an attempt was made to further investigate the "metallurgical notch" phenomenon postulated by Brucker.

II. EXPERIMENTAL PROCEDURE

A. MACRO SAMPLES

1. Preparation

The instrumented weld plate, measuring 30 inches (76.2 cm) by 40 inches (101.6 cm) was torch cut at MINSY to facilitate transportation and handling. The cuts were made parallel to and approximately 4 inches (30.16 cm) from the weld centerline. The plate was then sectioned perpendicular to the weld with a horizontal band saw into approximately three-quarter inch (19.05 mm) thick specimens. Each specimen contained two thermocouples, one on each side of the plate. A diagram of a typical macro sample appears as Figure 1. The faces of the specimens were then surface machined to just penetrate the holes containing the thermocouples. The faces were then sanded on a belt sander using 180 grit then 240 grit paper to remove the machining marks and to produce a smooth, flat surface suitable for macro etching. A solution of 10 grams of ammonium persulphate in 90 milliliters of distilled water proved to be the best macro etchant and revealed characteristics of the HAZ which were not visible with a concentrated sulfuric acid etchant (Fig. 2). The ammonium persulphate etch was used successfully by Stoop and Metzbower [Ref. 13] and by Connor and Haak [Ref. 14] to reveal the characteristics of the HAZ in various steel weldments. The surface of each macro sample

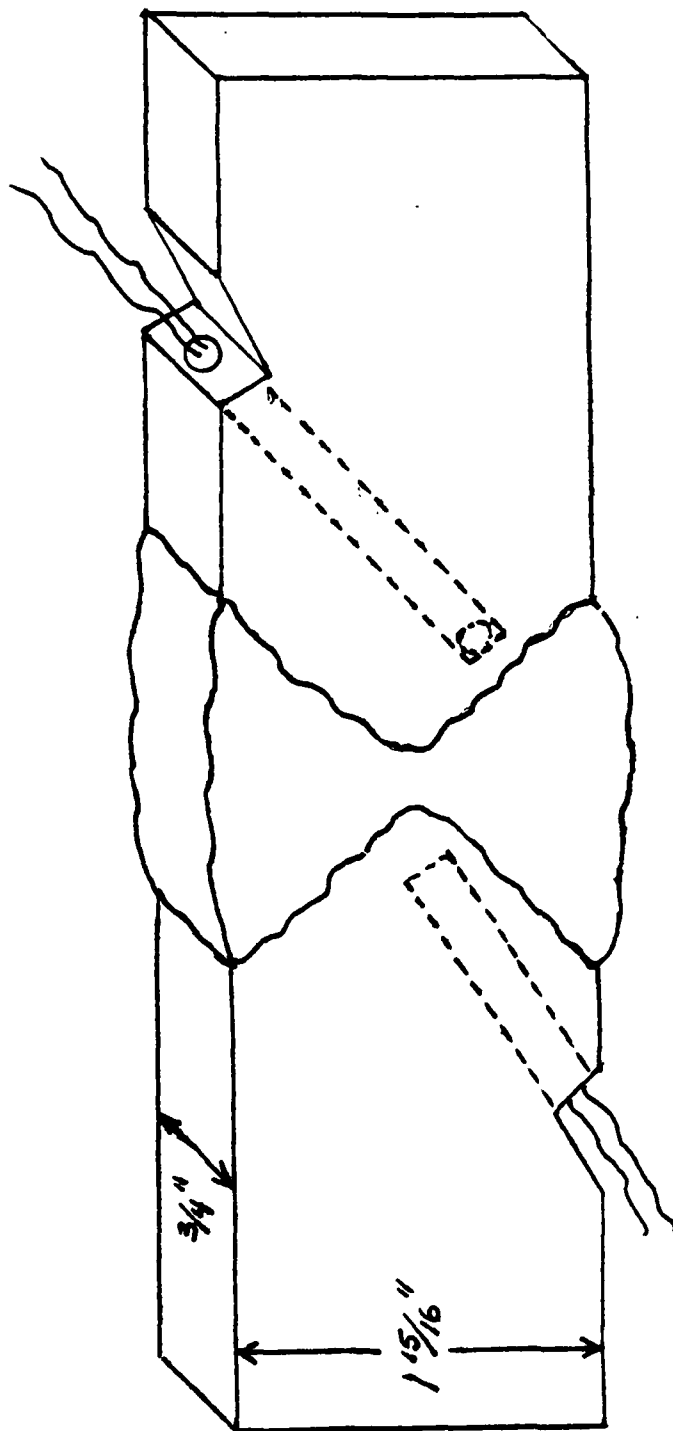


Figure 1. Macro sample of welded plate showing thermocouple placement.



Figure 2. Example of resolution of weld area possible with ammonium persulphate etch.

was alternately swabbed with the ammonium persulphate solution using a cotton tipped applicator and rinsed with distilled water until the desired degree of contrast was obtained. Photographs were taken of each macro sample and are presented as Figures 3 through 12. Note that a temper bead sequence was used on the top half of the weld and a straight sequence used on the bottom half.

2. Physical Measurements

At each thermocouple location, measurements were made of the distance from the bottom of the thermocouple hole to the fusion line of the weld and to the edge of the visible HAZ. Measurements were also made of the thickness of the visible HAZ in the vicinity of the thermocouple hole. All of these measurements were made using a Bausch & Lomb 7X surface observation lens containing a calibrated scale with 0.1 mm divisions.

These measurements were made in order to determine the location of the thermocouple with respect to the fusion line after welding and to permit comparison of the physical characteristics associated with the thermocouples.

B. METALLOGRAPHIC SAMPLES

Samples of a suitable size for metallographic examination were cut from the macro specimens using a high speed Do-All diamond saw. Each specimen contained the metal surrounding only one thermocouple attachment point. The specimens were then mounted on edge in Bakelite, using standard metallographic



Figure 3. Location of thermocouple 1-1.



Figure 4. Location of thermocouple 1-2.



Figure 5. Location of thermocouple 1-3.

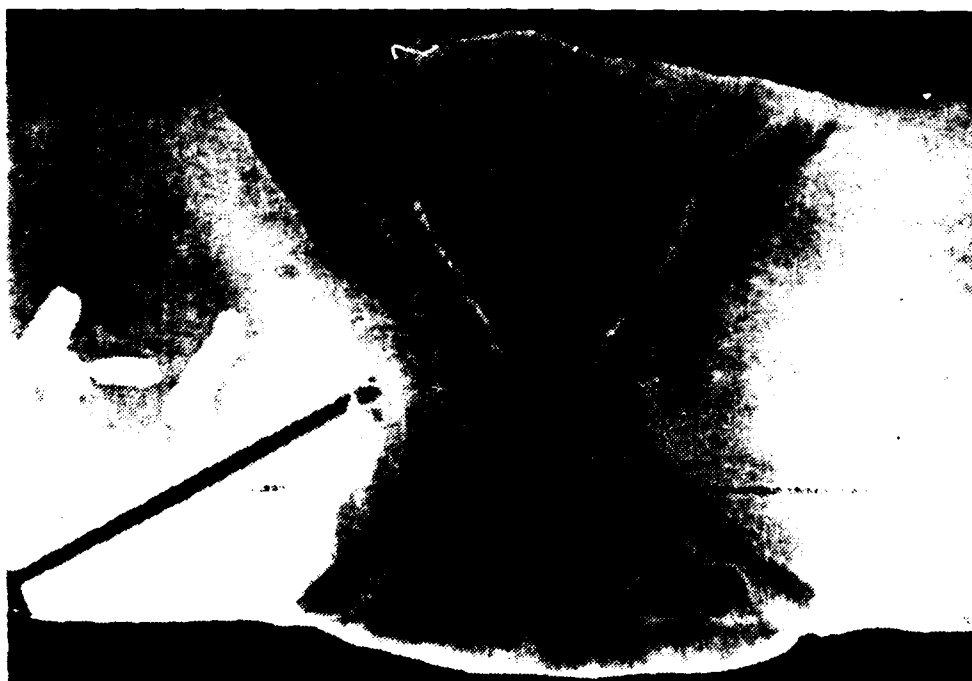


Figure 6. Location of thermocouple 1-4.



Figure 7. Location of thermocouple 2-1.



Figure 3. Location of thermocouple 2-2.



Figure 9. Location of thermocouple 3-2.



Figure 10. Location of thermocouple 3-3.



Figure 11. Location of thermocouple 3-4.

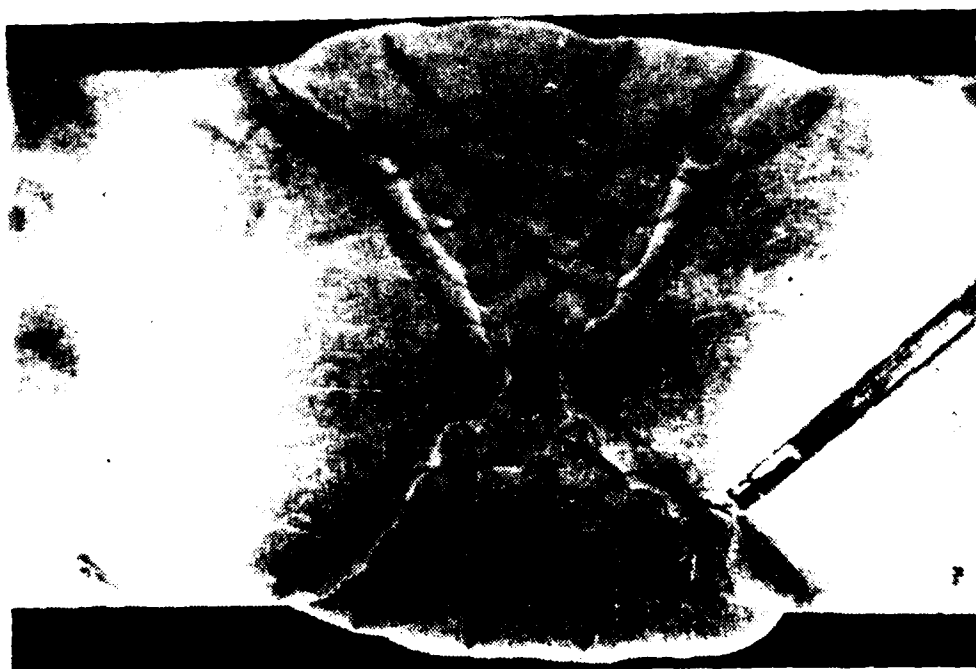


Figure 12. Location of thermocouple 4-1.

sample preparation techniques, to permit microscopic examination at the precise point of the thermocouple attachment. Extreme care was taken during subsequent grinding and polishing to ensure that the surface presented was in fact that of the point of attachment of the thermocouple and not below it. This was considered critical as the peak temperatures experienced during welding were found to vary widely over distances as small as one-eighth of an inch (3.17 mm). The samples were then etched by immersion in a 5% nital solution and examined with a Zeiss Universal Photomicroscope. Photographs were taken at selected thermocouple locations in an attempt to characterize the microstructure present.

C. HARDNESS MEASUREMENTS

To aid in the determination of the degree of tempering achieved at each of the thermocouple locations, a microhardness traverse consisting of five penetrations was conducted in the area of the thermocouple attachment point on each of the metallographic samples.

One macro specimen, cut from the plate in an area between thermocouple locations, was prepared for macro-etching in the same way as the others. After etching with the ammonium persulphate solution, this sample was tested using a Wilson Rockwell Hardness Tester with a Brale indenter and a 150 kilogram load. Penetrations were made at 0.1 inch (2.54 mm) intervals. A total of 5 linear traverses were made on the sample. A diagram of the traverse locations appears as Figure 13.

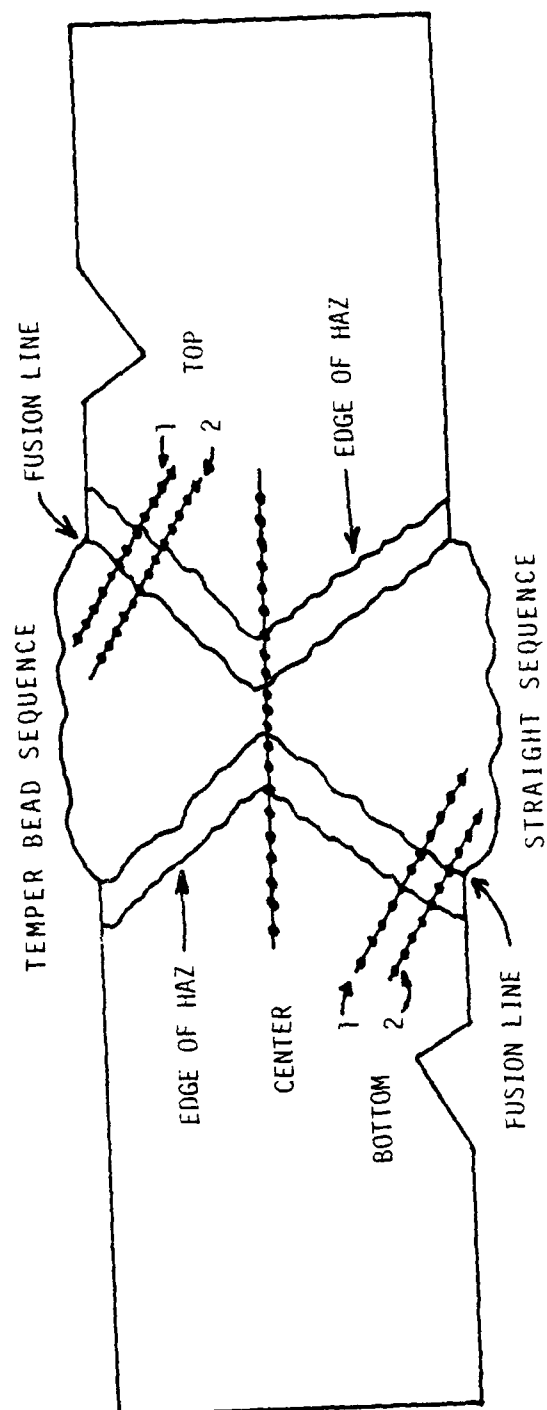


Figure 13. Diagram of Rockwell hardness traverse locations.

The macro sample containing thermocouples 1-3 and 3-3 was cut using the high speed diamond saw to produce one metallographic sized specimen from the area of the last pass of the straight sequence welded side of the plate and two specimens from the corners of the temper bead sequence. A diagram of the specimen locations appears as Figure 14. Each of the specimens was mounted in Bakelite, polished and etched with the ammonium persulphate solution. Microhardness traverses were conducted on each sample perpendicular to the fusion line at 50 micron intervals using a diamond pyramid indenter and a 200 gram load. Figures 15a, b, c, indicate the locations of these traverses. A total of 4 linear traverses were made with an average of approximately 100 penetrations per traverse.

D. ANALYSIS OF THE TIME-TEMPERATURE PLOTS

The time-temperature plots were examined to determine the peak temperature each thermocouple experienced during each weld pass. Determination of the peak temperature was accomplished by first preparing a temperature scale using the data collected during a calibration run of the instrumentation prior to the commencement of the welding. Calibration data were available for temperatures of 70, 500, 750, 1000, 1250, 1500, 1750, 2000 and 2288°F. When plotted, the data produced a nearly linear scale. As no additional information was available as to the nature of the non-linearity, it was decided to approximate the temperatures between the known data points by linear interpolation

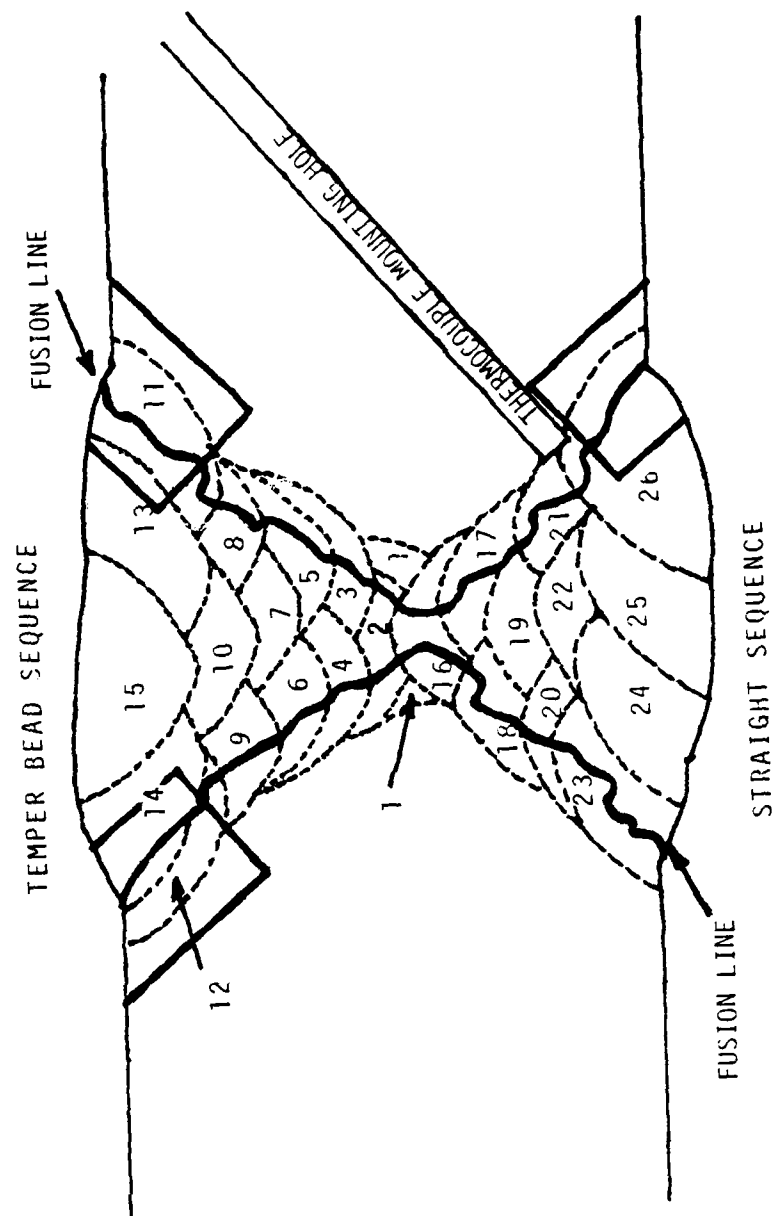
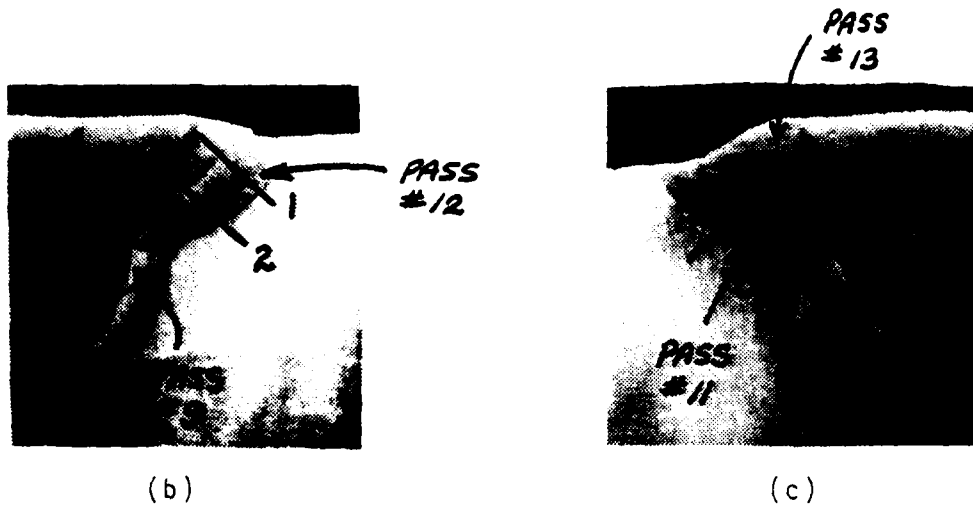


Figure 14. Diagram of micro specimen cutting locations.



(a)



- Legend:
- (a) Last pass, straight sequence
 - (b) Pass #9,12, temper bead sequence
 - (c) Pass #11,13, temper bead sequence

Figure 15. Locations of microhardness traverses.

methods. It is recognized that some error in the measurement of the temperatures is thus introduced. However, the error is estimated to be less than 8°F.

The time to reach a given temperature during both heating and cooling of the weld area was measured and recorded for later use in determining the tempering parameter P. Typical time-temperature plots are presented as Figures 16 and 17.

E. CALCULATION OF THE TEMPERING PARAMETER

In addition to the temperature measurement, it was desired to determine the amount of tempering each thermocouple location experienced due to previous and subsequent weld passes. To determine the amount of tempering a given area received, the tempering parameter P for that location was calculated using equations developed by Hollomon and Jaffee [Ref. 15].

For the initial tempering due to the rise from the preheat/maximum interpass temperature of 250°F to one-half the peak temperature, equation (1) was used.

$$P_s = T (c + \log t) \quad (1)$$

where: T = temperature, °K

t = time spent at temperature T, in seconds

c = constant

For these calculations, the simple average of 250°F and one-half the peak temperature, converted to °K, was used as an approximation for T and the time elapsed during the rise from 250 °F to one-half the peak temperature

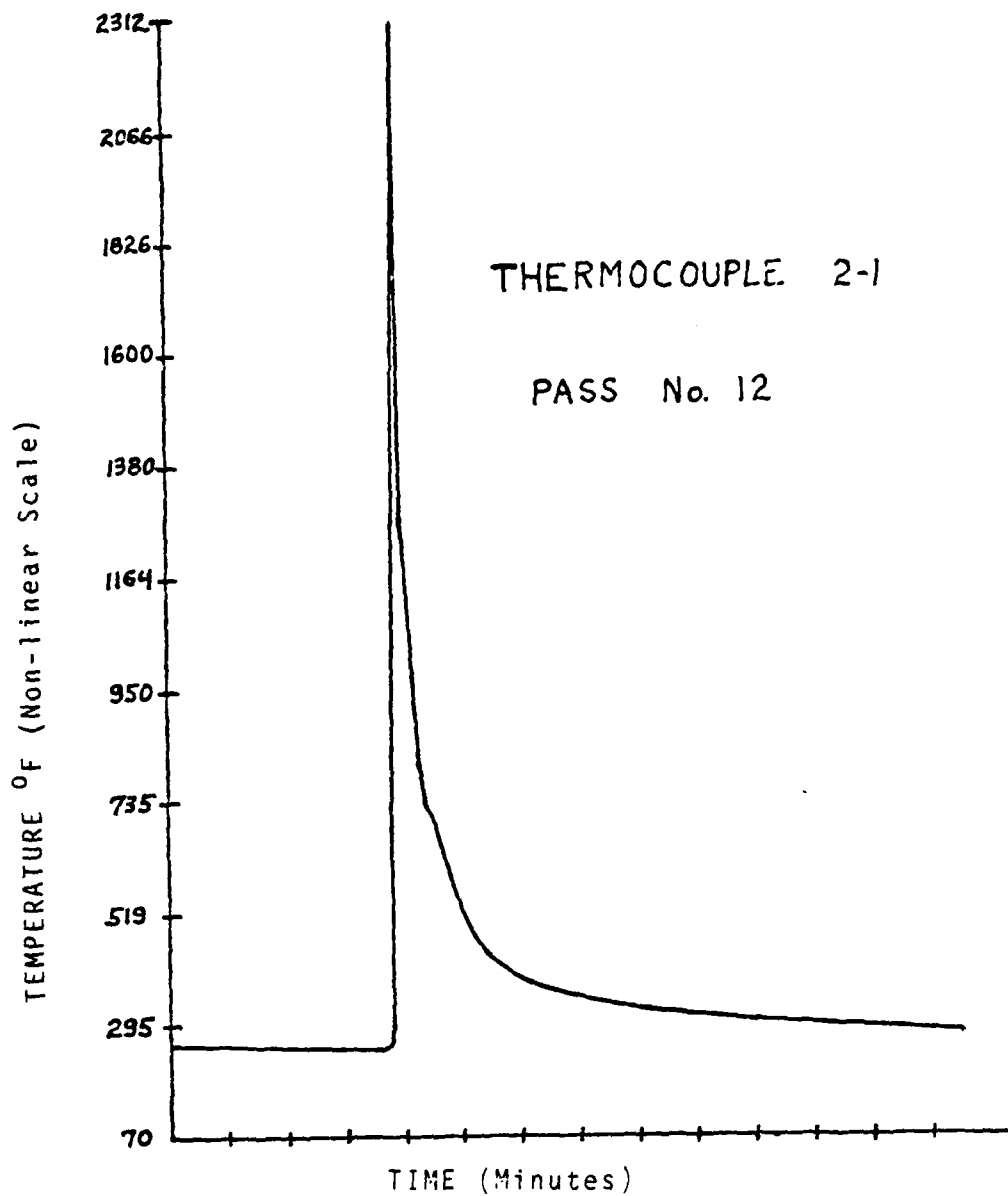


Figure 16. Time-Temperature Plot for
Thermocouple 2-1, Pass 12

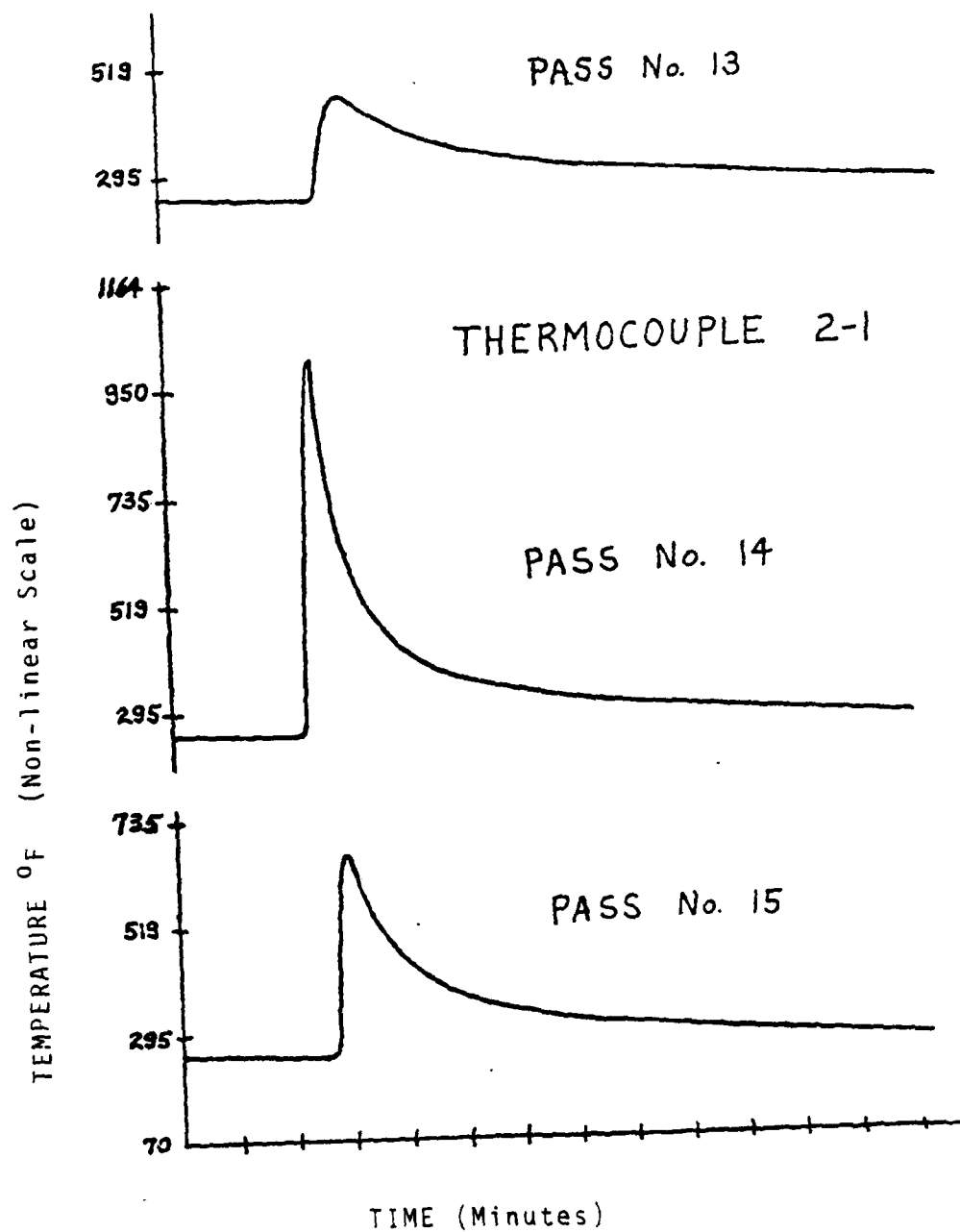


Figure 17. Time-Temperature Plot for
Thermocouple 2-1, Passes 13, 14, 15

was used as an approximation for t . The value of one-half the peak temperature was arbitrarily chosen to provide two values for T during the rise to the peak temperature, increasing the accuracy of the estimate. Further subdivision of the rising portion of the time-temperature plot was impossible as the time intervals became too small to accurately measure.

To determine the increase in the magnitude of the tempering parameter due to the remainder of the thermal cycle, equation (2) was used.

$$P = T \log \left(\frac{\Delta t}{10^{-c}} + 10^{\frac{P_s}{T}} \right) \quad (2)$$

where: T = new higher or lower temperature, $^{\circ}\text{K}$

Δt = time spent at the new temperature, in seconds

P_s = initial value of the tempering parameter, from equation (1)

c = constant

For these calculations the temperature T was taken as the simple average between the following values (when applicable) converted to $^{\circ}\text{K}$:

1/2 Peak Temperature	and	Peak Temperature
Peak Temperature	and	720 $^{\circ}\text{F}$
720 $^{\circ}\text{F}$	and	600 $^{\circ}\text{F}$
600 $^{\circ}\text{F}$	and	500 $^{\circ}\text{F}$
500 $^{\circ}\text{F}$	and	400 $^{\circ}\text{F}$
400 $^{\circ}\text{F}$	and	300 $^{\circ}\text{F}$
300 $^{\circ}\text{F}$	and	250 $^{\circ}\text{F}$

The time value, Δt , was taken as the time elapsed during the rise/fall between the temperatures listed above. The value of the constant, c , was chosen to be 14.44 following the work done by Grange and Baughman [Ref. 16]. They used a similar approach in the calculation of the tempering parameter and used a value of 18.0 for the constant c for a wide range of steels and concluded that the value of the constant was not critical. In their calculations the time t was expressed in hours. A corresponding value of $c = 14.44$ is obtained when time is expressed in seconds in equations (1) and (2), and it was decided to use this value for the constant c in all of the calculations in this research.

The value of 720 degrees Fahrenheit is also of particular interest. Research conducted by United States Steel Corporation's Applied Research Laboratory [Ref. 16] on HY-130 steel has resulted in the development of an isothermal transformation diagram and the determination of the approximate A_1 , A_3 , and M_s temperatures for this steel. A reproduction of this diagram appears as Figure 18. The M_s temperature is approximately 720°F (382°C) and the A_1 temperature is approximately 1210°F (655°C). The A_3 temperature has been determined to be approximately 1400°F (760°C) [Ref. 17]. Determination of the time elapsed during cooling from the peak temperature to 720°F (382°C) would be useful in determining whether transformation from austenite to martensite had occurred.

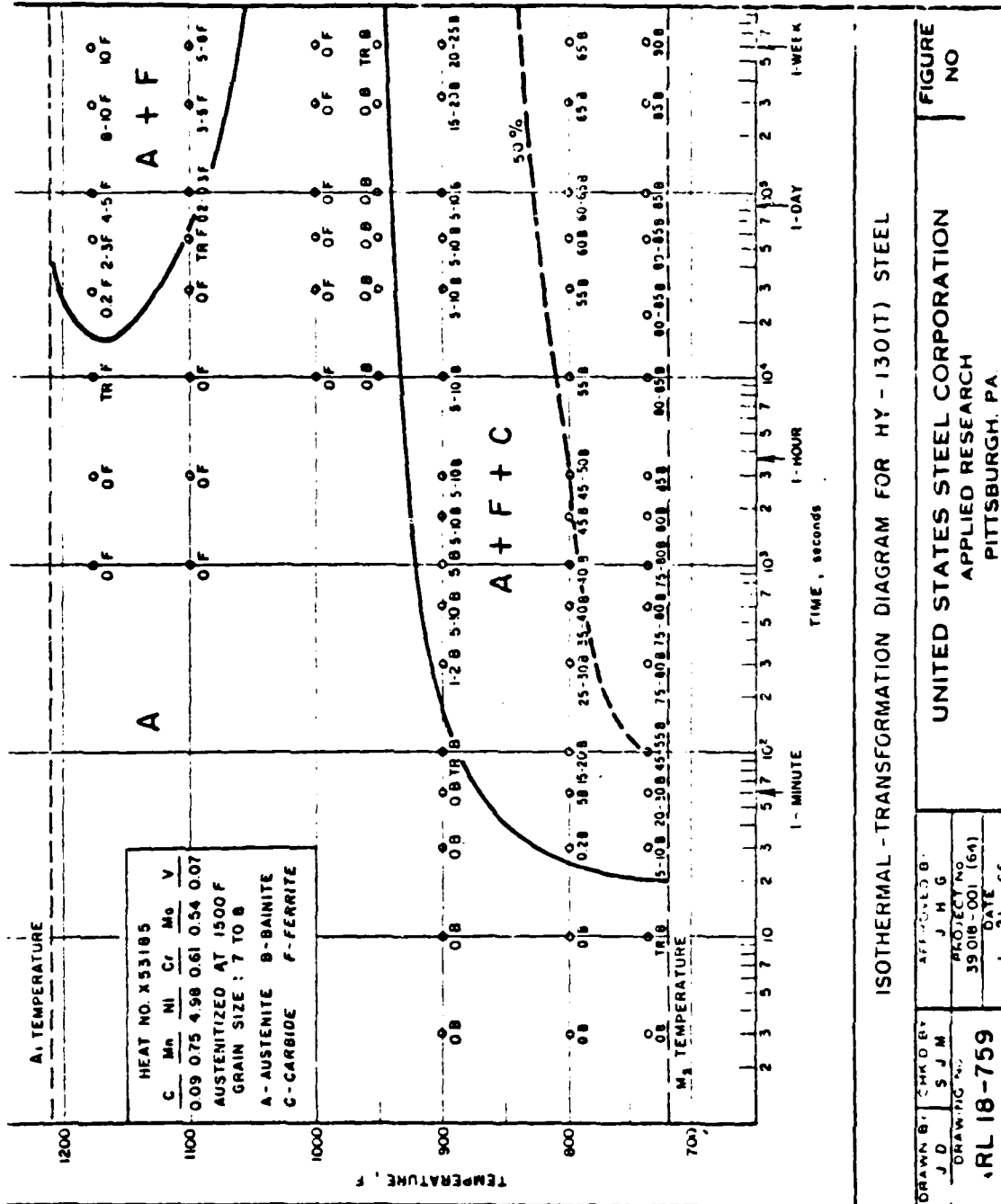


Figure 18

F. CARBON EXTRACTION REPLICAS

Following optical metallography, each of the metallographic specimens was re-polished using a 1.0 micron diamond paste and re-etched by immersion in a 5% Nital solution. The samples were then placed, one at a time, in a Fullam Model 1250 vacuum evaporator where a thin film of carbon was deposited on the surface of each. Deposition was accomplished with the vacuum in the chamber at 6×10^{-5} torr. A current of 50 amps was passed through the carbon electrodes for a burn time of approximately three seconds. The surface of each sample was then scribed to form a 2 millimeter grid pattern at the location of the thermocouple attachment point and immersed in a 10% Nital solution to remove the replica from the surface. The samples were then immersed in a 2% Ethanol in distilled water solution to float the replica from the sample. The replicas were then captured on a 3 millimeter diameter copper grid and allowed to dry. Examination and photography of the replicas was performed on a Phillips Model EM 201 Transmission Electron Microscope (TEM) at Stanford University's Hopkins Marine Station in Pacific Grove, California.

III. RESULTS AND DISCUSSION

A. MACROSCOPIC EXAMINATION

The results of the physical measurements of the base metal HAZ width and the distance from the fusion line to each thermocouple attachment point are presented in Table II. Also included are the distances of the thermocouples from the beveled weld groove prior to welding. The average width of the base metal HAZ was found to be 0.16 inches (3.95 mm) and did not vary significantly with location on the plate or with the weld bead sequence used. Figure 19 shows the peak temperature recorded by the thermocouple plotted versus its distance from the fusion line after welding. The scatter in the data presented is due to the uncertainty in the position of the thermocouple at the bottom of the hole in the welded plate. The holes were 0.25 inches in diameter (6.35 mm). As can be seen in the inset in Figure 19, one corner of the hole shown is closer to the fusion line (traced) than the other. If the thermocouple were located at this corner, it would indicate a higher peak temperature for the nearest weld pass than if mounted at any other location on the bottom of the hole. A similar argument can be made for all thermocouple locations. Since the thermocouple wires were mounted in an insulating ceramic sleeve which tended to center the wires in the hole, it is estimated that 95% were within 0.07 inches (1.78 mm)

TABLE II

Physical Data for Selected Thermocouple Locations


THERMOCOUPLE NUMBER	PEAK TEMPERATURE (°F)	A	B	C	D	E	F	G
1-4	771	7.2	7.7	11.5	12.5	12.70	4.0	TB
3-4	696	8.6	8.6	11.0	12.4	13.97	4.0	S
1-3	1062	2.6	3.2	7.2	7.25	8.89	3.8	TB
3-3	833	4.7	6.2	6.5	8.4	10.16	3.8	S
1-2	1424*	IN HAZ	IN HAZ	3.9	3.9	5.08	4.0	TB
2-2	1250	EDGE OF HAZ	EDGE OF HAZ	3.0	4.2	5.08	4.0	TB
3-2	893	1.0	1.0	4.1	5.6	6.35	4.0	S
2-1	2301	IN HAZ	IN HAZ	0.0	1.0	2.03	4.0	TB
4-1	2242	IN HAZ	IN HAZ	0.4	0.4	3.05	4.0	S

*Temperature used here is that of second pass as first (or root) pass was completely re-melted by second.

KEY: A - Distance from thermocouple to nearest part of HAZ (mm).

B - Distance from thermocouple to HAZ  to bottom of hole (mm).

C - Distance from thermocouple to nearest part of fusion line (mm).

D - Distance from thermocouple to fusion line  to bottom of hole (mm).

E - Distance from thermocouple to weld bevel before welding (mm).

F - Average HAZ thickness at thermocouple location (mm).

G - Weld sequence used (S = straight, TB = temper bead).

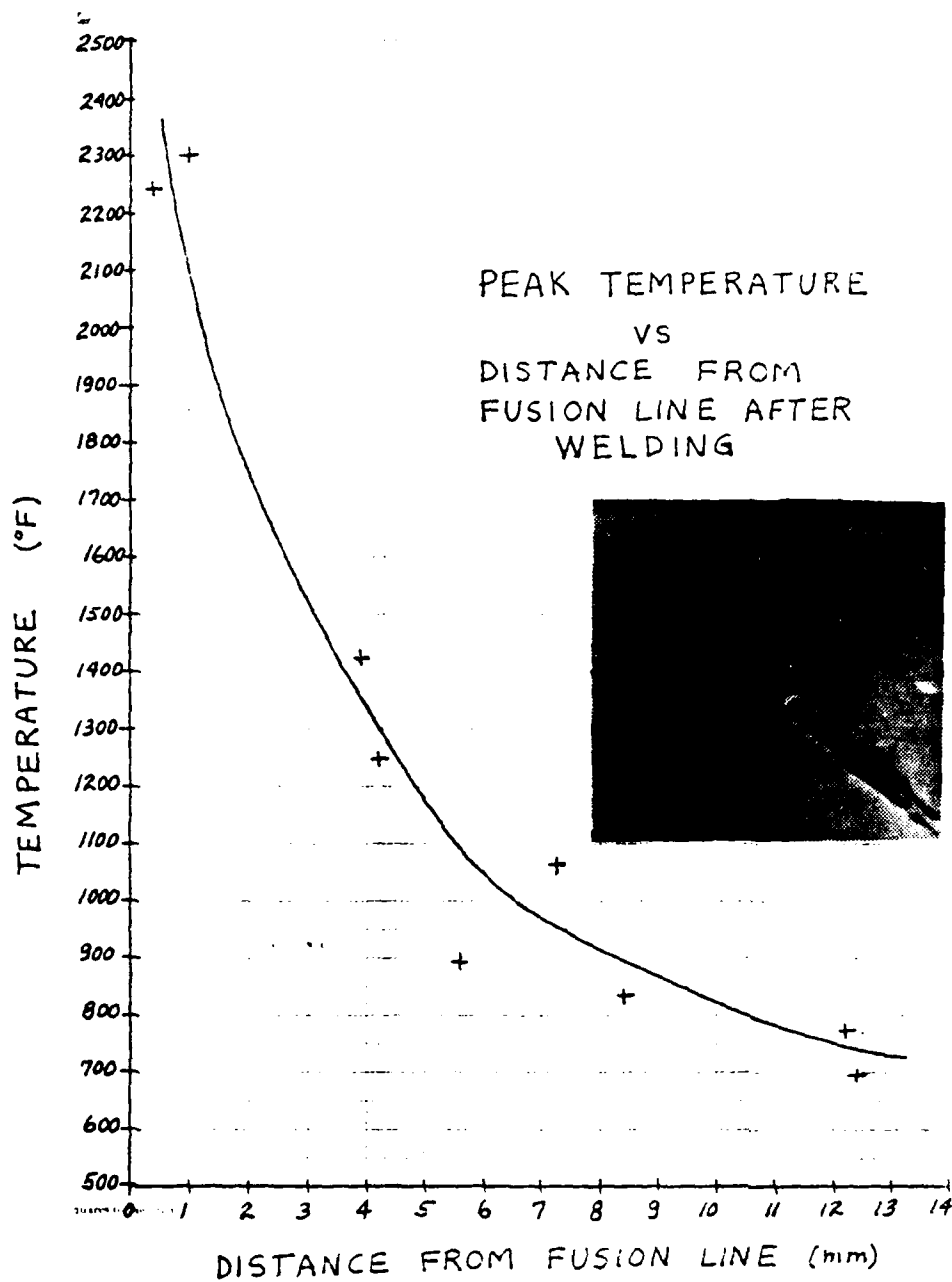


Figure 19. Peak Temperature vs. Distance From Fusion Line After Welding

of the hole center, assuming a normal distribution. A determination of the error in the measurement of the temperature as a function of distance from the fusion line is rendered difficult by the dew drop shape of the weld bead as depicted in the inset of Figure 19. The magnitude of the error would increase as the distance from the fusion line decreased due to the steepness of the temperature gradient in that region.

B. ROCKWELL HARDNESS MEASUREMENTS

The results of the Rockwell hardness traverses conducted are presented in Tables III, IV and V. It should be noted that the HAZ region hardness on both the temper bead side of the plate and in the center of the plate is about 3 R_C lower than the HAZ on the straight sequence side. The weld metal hardness near the fusion line was also higher for the straight sequence side of the plate.

These measurements are not considered conclusive in any way. They do, however, indicate a trend which was later verified by microhardness traverses. The Rockwell hardness test, due to the relatively large size of the indentations it produces, is not suited for measurement intervals closer than 0.1 inch (2.54 mm).

C. MICROHARDNESS MEASUREMENTS

The microhardness traverses conducted as described in the experimental procedure section of this report produced the results indicated in Figures 20, 21, 22 and 23. Particularly noteworthy is the rapid drop in hardness shown for the last

TABLE III

Rockwell Hardness Data, Temper Bead Sequence

	TOP #1		TOP #2	
	DISTANCE FROM FUSION LINE (INCHES)	HARDNESS ROCKWELL "C"	DISTANCE FROM FUSION LINE (INCHES)	HARDNESS ROCKWELL "C"
WELD METAL			.4	29.8
	.3	28.3	.3	28.8
	.2	33.9	.2	34.2
	.1	36.6	.1	35.5
	FUSION LINE	38.2	FUSION LINE	38.1
	.1 (HAZ)	34.5	.1 (HAZ)	33.7
	.2 (HAZ)	33.0	.2	29.9
	.3	32.5	.3	31.1
	.4	31.8	.4	31.6
	.5	31.2	.5	31.2
BASE METAL	.6	30.6	.6	30.2

TABLE IV

Rockwell Hardness Data, Root of the Weld

CENTER LINE (ROOT OF WELD)		
	DISTANCE FROM FUSION LINE (INCHES)	HARDNESS ROCKWELL "C"
BASE METAL RIGHT SIDE	.7	30.2
	.6	30.0
	.5	29.6
	.4	30.2
	.3	31.6
	.2 (HAZ)	30.5
	.1 (HAZ)	34.9
	FUSION LINE	37.5
WELD METAL	.1	29.8
	FUSION LINE	32.8
	.1 (HAZ)	36.0
	.2 (HAZ)	28.2
	.3	31.0
LEFT SIDE BASE METAL	.4	30.2
	.5	29.8
	.6	29.2
	.7	28.3

TABLE V

Rockwell Hardness Data, Straight Bead Sequence

	BOTTOM #1		BOTTOM #2	
	DISTANCE FROM FUSION LINE (INCHES)	HARDNESS ROCKWELL "C"	DISTANCE FROM FUSION LINE (INCHES)	HARDNESS ROCKWELL "C"
WELD METAL			.3	35.8
	.2	36.8	.2	37.5
	.1	37.8	.1	37.6
	FUSION LINE	37.0	FUSION LINE	38.0
	.1 (HAZ)	38.0	.1 (HAZ)	38.5
	.2 (HAZ)	32.1	.2	32.0
BASE METAL	.3	31.0	.3	30.9
	.4	30.0	.4	29.5
	.5	30.5	.5	29.4
	.6	30.1	.6	29.3

pass of the straight sequence welded side of the test plate (Fig. 20), occurring at approximately 3.5 millimeters from the fusion line. This sharp drop occurs near the edge of the HAZ farthest from the fusion line and confirms a finding by Brucker [Ref. 18] supporting the theory that a "metallurgical notch" was produced in the HAZ by the welding process. The drop in hardness from an average of 400 to a low of 275 on the Vickers scale corresponds to a drop in yield strength from approximately 188 ksi to 125 ksi. The rapid drop is seen to occur over a distance of only 0.25 mm (0.01 inch).

Figure 21 represents the results of the microhardness traverse located as shown in Figure 15c. Figure 15c clearly indicates two HAZ's in the area of the hardness traverse. The initial drop in hardness from an average of 370 to an average of 340 on the Vickers scale occurs at a distance of approximately 1.5 millimeters from the fusion line. This corresponds to the limit of the HAZ produced by the thirteenth weld pass. The second sharp decrease in hardness similarly corresponds to the limit of the HAZ produced by the eleventh weld pass. The fine grained region of the HAZ produced by the eleventh pass was not re-austenitized by the thirteenth pass, but was tempered by it. The coarse grained region of the eleventh pass HAZ was re-austenitized by the thirteenth pass at a lower peak temperature (than experienced during the eleventh pass) resulting in an extremely fine microstructure which was tempered by the final pass. Studies by Kellock, et al, [Ref. 19]

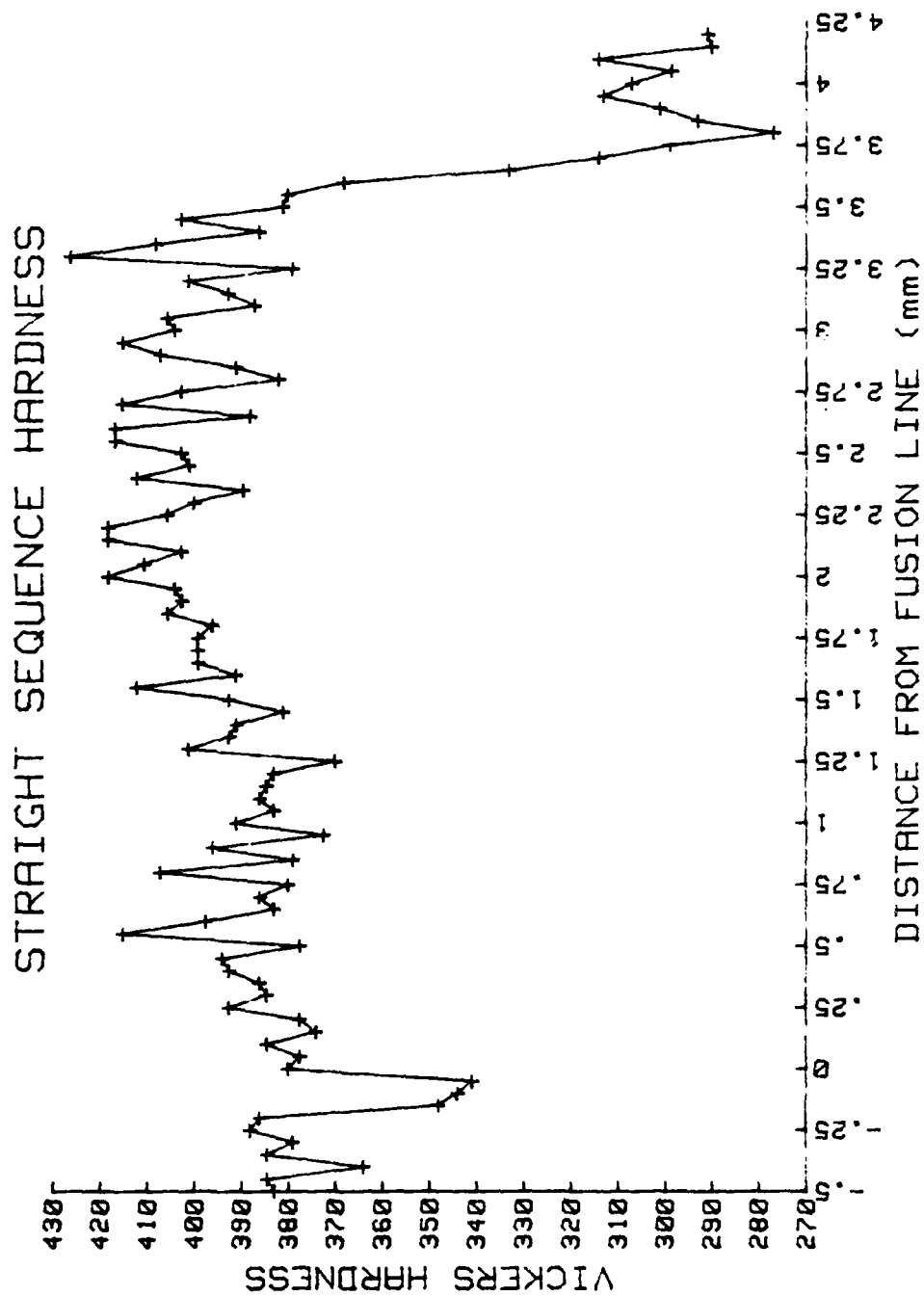


Figure 20. Microhardness Traverse Results for Location Indicated in Figure 15a.

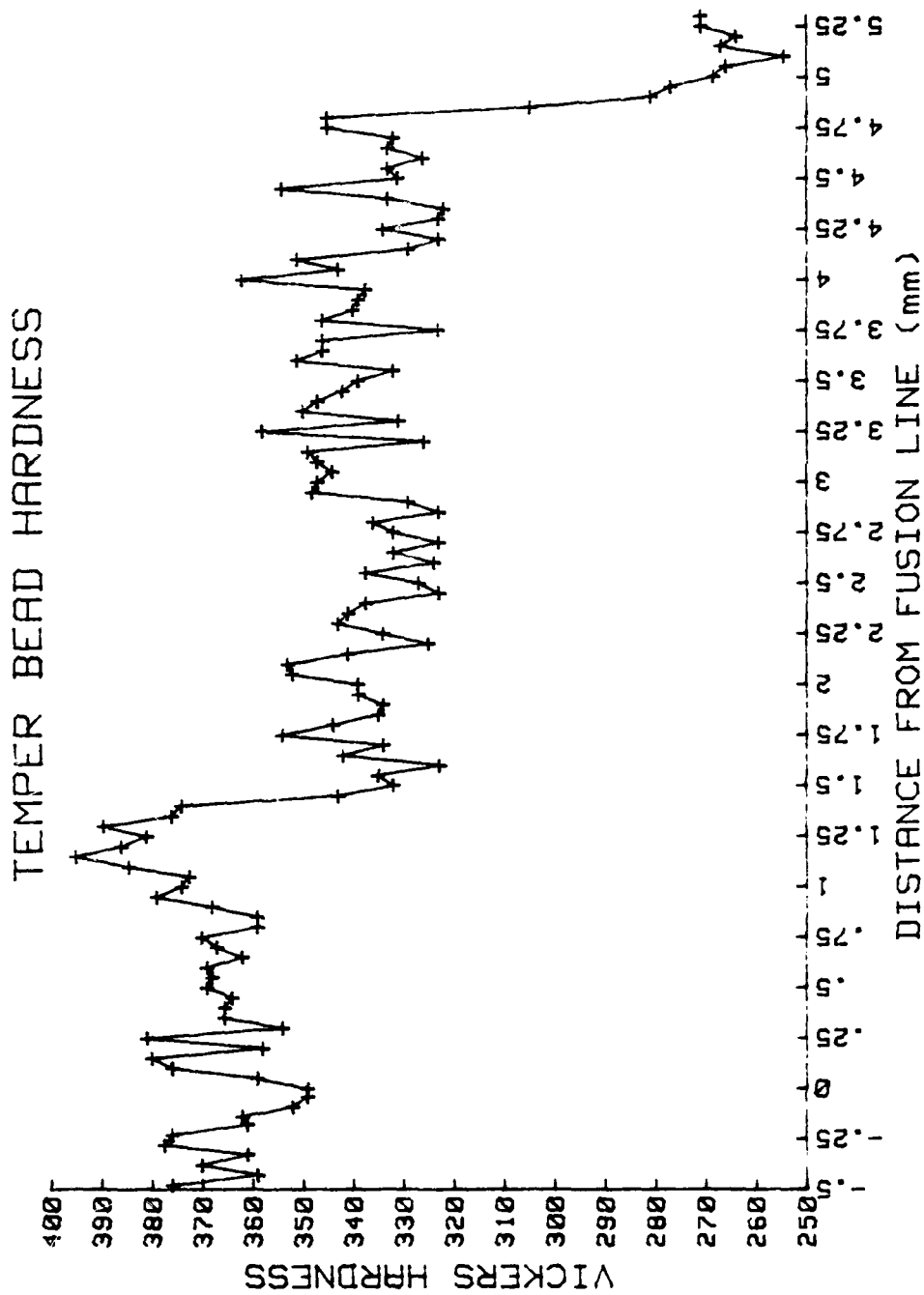


Figure 21. Microhardness Traverse Results for Location Indicated in Figure 15c.

of simulated weld HAZ structures and properties in HY-80 steel indicated nearly identical results for that alloy when subjected to a similar thermal history.

Figure 22 is a plot of the results of the microhardness traverse conducted at the location shown in Figure 15b(1) on the temper bead side of the plate. The shape of this plot is similar to that of Figure 20, but there are some important differences. The drop in hardness measured at this location is from an average of 370 to 270 on the Vickers scale. This corresponds to a change in yield strength from approximately 166 ksi to 125 ksi. The decline is also more gradual, occurring over a distance of approximately 0.5 millimeters (0.02 inch). The reduction in the hardness gradient is due to the effect of tempering caused by subsequent weld passes. Kellock, et al [Ref. 20] reported similar changes in hardness in the HAZ of HY-80 steel due to tempering. Thus the tempering produced by subsequent weld passes reduces the severity of the "metallurgical notch" by lowering the average hardness of the HAZ from about 400 to about 370 on the Vickers scale and increasing the distance over which the change occurs from 0.25 millimeters to 0.5 millimeters (0.01 inches to 0.02 inches).

Figure 23 represents the results of the microhardness traverse located in closely overlapping HAZ's resulting from the ninth and twelfth weld passes as shown in Figure 15b(2). The hardness in the area from the fusion line through approximately one-half the total width of the base metal HAZ is

TEMPER BEAD HARDNESS

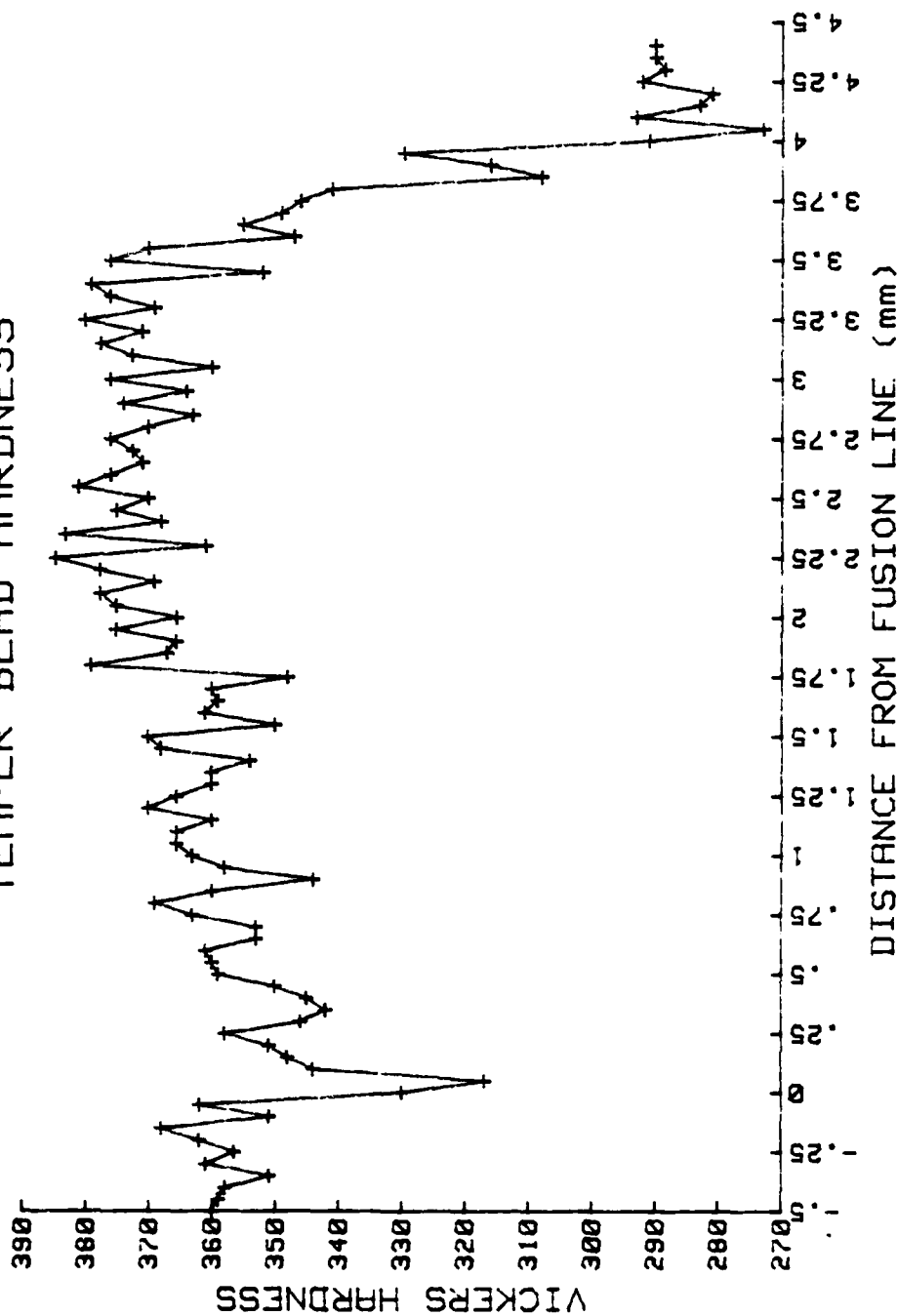


Figure 22. Microhardness Traverse Results for Location Indicated in Figure 15b (1).

TEMPER BEAD HARDNESS

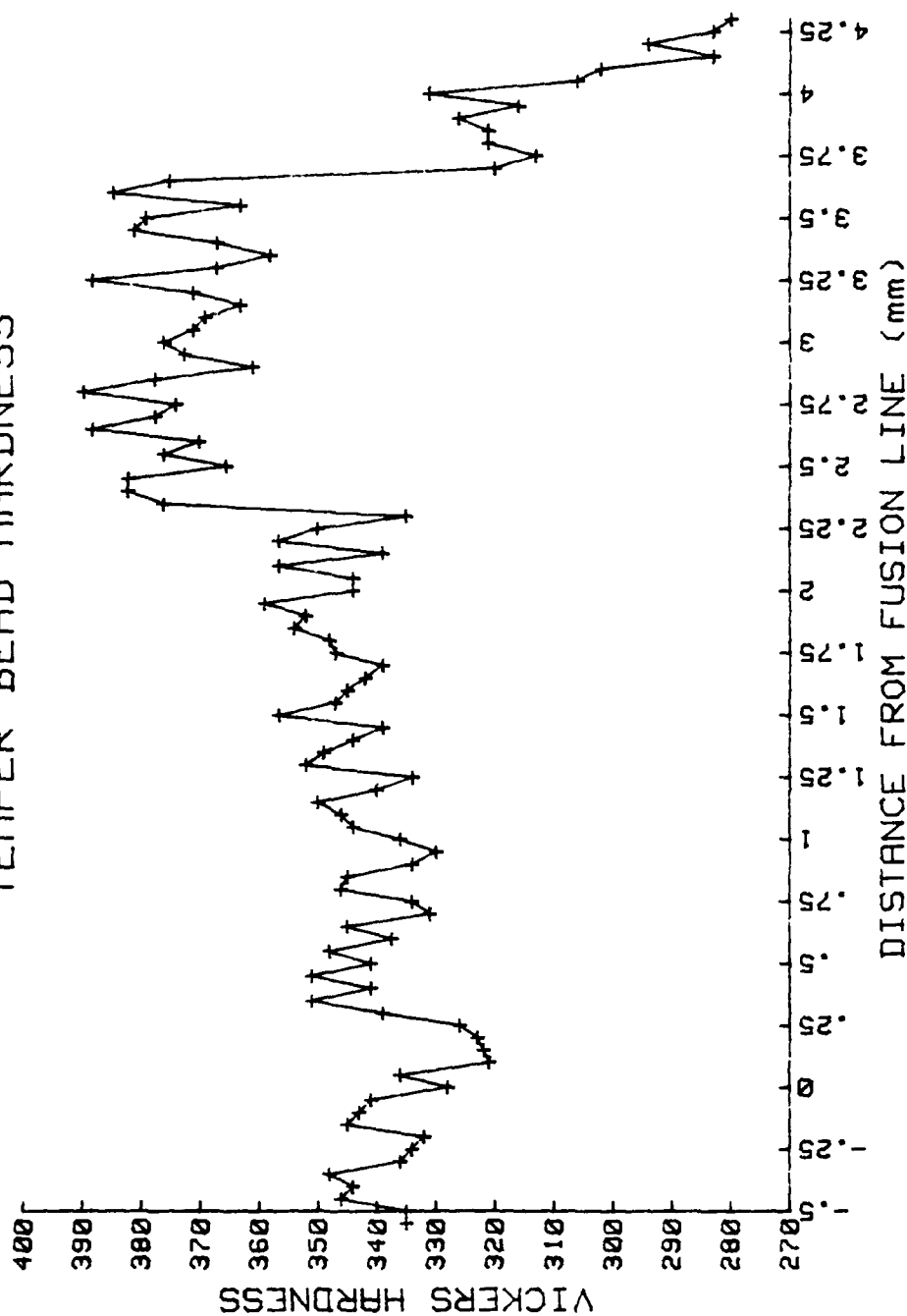


Figure 23. Microhardness Traverse Results for Location Indicated in Figure 15b (2).

similar to that found in a corresponding region of the base metal HAZ in the first traverse made on that sample (Fig. 15b(1)). The region of higher hardness, averaging 370 on the Vickers scale corresponds to that area of the HAZ produced by the ninth weld pass which was heated into the intercritical temperature range and subsequently heated again into the intercritical range by the twelfth weld pass. The carbon content of austenite formed as a result of heating in the intercritical temperature range will increase (above the nominal 0.1% carbon content) as the austenitizing temperature decreases. Thus, the martensite formed upon cooling from low intercritical temperatures will have a higher hardness than martensite formed upon cooling from higher austenitizing temperatures. The amount of martensite produced, however, will decrease as the austenitizing temperature is decreased within the intercritical temperature range. The measured hardness then, represents the average hardness of the ferrite-carbide-martensite mixture. This average hardness is similar for all austenitizing temperatures within the intercritical temperature range. In all of the locations examined in this research, the region of the HAZ that was austenitized in the intercritical temperature range exhibited a higher hardness than those regions which were austenitized at higher temperatures. The location at which this change in hardness occurs is coincident with a change from a very fine microstructure (probably that of the mixture of ferrite, carbides, and

martensite discussed above) to a much coarser martensitic microstructure. A trend is also seen to exist in the coarse grained region of the HAZ, where the measured hardness increases as the microstructure becomes finer.

Austenitizing in the intercritical temperature range (as discussed later in the section of this report concerning microstructural analysis) does not dissolve all of the carbides present in the initial tempered martensitic structure. A double austenitizing treatment, such as that experienced at thermocouple location 1-2 and in the vicinity of the microhardness traverse shown in Figure 15b(2), dissolves more of the carbides and results in a higher hardness. Austenitizing at a temperature in excess of the A_3 temperature was found to dissolve all of the carbides in the initial tempered martensitic structure. A double austenitizing treatment at a temperature above the A_3 temperature would thus not be expected to produce a change in the hardness. It is believed that the closely overlapping HAZ's produced by the ninth and twelfth weld passes are responsible for the more substantial increase in hardness observed at the fine grain/coarse grain HAZ boundary, than observed at any of the other locations examined.

The small area between about 3.6 millimeters (0.14 inches) and 4.0 millimeters (0.16 inches) from the fusion line, with an average hardness of approximately 320 on the Vickers scale is that region of the HAZ produced by the ninth weld pass which was not re-austenitized by the twelfth weld pass. This

region was subjected to some tempering from the twelfth weld pass resulting in a lower hardness than recorded for any other portion of the base metal HAZ. The tempering of the entire HAZ by subsequent weld passes accounts for the fact that the peak hardness is lower than that recorded for the straight sequence final pass HAZ.

It should be noted that in all cases, the fusion line hardness is much lower than that of either the adjacent weld metal or the adjacent base metal HAZ. The microhardness traverses also indicate a trend in increasing hardness as the measurements proceed from the fusion line through the HAZ. This increase is slight and is evident in both the straight sequence and the temper bead sequence hardness traverses presented in Figures 20 and 22.

The results of the microhardness measurements made at the thermocouple attachment points are presented in Table VI. As is evident from the data shown in the table, there is a significant difference in the hardness measured at different thermocouple locations, from a low of 291 to a high of 382 on the Vickers hardness scale. This corresponds approximately to a change from 30 to 40 on the Rockwell "C" scale. The variations in hardness measurements were not unexpected. Thermocouple 4-1 exhibited the highest hardness value which is consistent with other results obtained in this research. At this location, the thermocouple experienced a final austenitizing pass which transformed the structure to martensite upon cooling. As this

TABLE VI
Microhardness Data for
Thermocouple Attachment Points

THERMOCOUPLE NUMBER	AVERAGE * VICKERS HARDNESS
1-4	303
3-4	298
1-3	291
3-3	302
1-2	360
2-2	347
3-2	334
1-1	313
2-1	335
4-1	382

*Statistical average of five readings.

location was that of the last pass on the straight sequence welded side of the plate, it did not receive any subsequent tempering by additional weld passes in the vicinity. The hardnesses for thermocouple locations most distant from the fusion line, 1-4, 3-4, 1-3 and 3-3, are very similar to one another and to the initial base metal values. This result was also expected as these four thermocouples were located in the base metal, at some distance from the HAZ. The readings obtained here would reflect essentially the hardness of the structure of the parent plate, that of tempered martensite. Thermocouples 1-2, 2-2 and 3-2 were located very near to the HAZ or within it and were subjected to varying amounts of re-austenitization and tempering during welding. The hardness values recorded for these thermocouples, as expected, were higher than those outside of the HAZ and lower than that of thermocouple 4-1. Thermocouples 1-1 and 2-1 were located in the HAZ at or very close (0.1 mm) to the fusion line. The hardness values recorded for these thermocouples reflects the hardness of the fusion line which was found to be lower than adjacent weld metal and the base metal HAZ.

D. THERMAL HISTORY ANALYSIS

The data obtained from the analysis of the time-temperature plots was used primarily to provide a basis for the investigation and correlation of hardness data and microstructural observations. Tables of the peak temperatures experience by

selected thermocouples during each weld pass along with the time recorded for the thermal cycles are presented in Appendix B.

The tempering parameter described in the experimental procedure section of this report was calculated for passes 3 through 15 at thermocouple location 1-2, and for passes 13, 14 and 15 at thermocouple location 2-1. These locations were chosen in order to compare the relative tempering effect due to the last three weld passes with that produced by a larger number of weld passes. The value of the tempering parameter calculated for the last three weld passes at thermocouple location 2-1 was $P = 11,613$ while that calculated for the large number of passes at thermocouple location 1-2 was $P = 11,871$. The difference in tempering effect produced at the two different thermocouple locations is therefore considered to be insignificant. In the course of the calculation of the total tempering parameter for each location, it was noted that the majority of the tempering effect is produced by the first weld pass immediately following the austenitizing pass. In the case of thermocouple location 1-2, the value of P as a result of pass number 3 was calculated to be $P = 9,722$. As a result of pass number 4, the total tempering parameter increased to $P = 11,870$, with only fractional increases contributed by each of the following eleven weld passes. Similarly, a value of $P = 8,009$ was calculated as the result of pass number 13 at thermocouple location 2-1 increasing to $P = 11,613$ after pass number 14.

The magnitude of the value of the tempering parameter, P , has only relative significance. It indicates the relative amount of tempering that is produced by different thermal histories, and once a value of the parameter has been calculated using the time-temperature data obtained from a complex thermal history as is the case here, it can be used in the reproduction of the same tempering effect by less complicated thermal histories. An identical value of P obtained by rapidly heating a sample of the same alloy, holding at a constant temperature for some time period, followed by cooling at a rate closely approximating that experienced by air cooling a thick section weldment, should produce identical tempering effects. This is especially useful in the laboratory production of simulated weld HAZ's of sufficient size for mechanical testing. The effects of simulated welds on the microstructure of HY-130 steel weldments is the subject of concurrent research conducted by Cincotta [Ref. 21].

E. MICROSTRUCTURAL ANALYSIS

The optical micrographs and photographs of the carbon extraction replicas produced during the course of this research are presented at the end of this section as Figures 24 through 33. They are arranged in order of decreasing distance from the fusion line of the weld and the discussion that follows will be similarly ordered.

1. Thermocouple Locations 1-4, 3-4

These two thermocouples were located at distances of 12.2 millimeters (0.48 inch) and 12.4 millimeters (0.49 inch) respectively from the fusion line after welding. The microstructures shown in Figures 24 and 25 are very similar and are representative of the base metal structure that existed prior to welding, that of tempered martensite. Located outside the HAZ, the microstructure in these areas would indicate little effect from the welding process. The carbon extraction replicas made at these locations are also indicative of the tempered martensitic structure, showing evidence of larger coarse carbides intermixed with finer carbide particles. The microhardness measurements made at these thermocouple locations (Table VI) agree with the Rockwell hardness measurements made on the base metal (Tables 3, 4, 5) further indicating a negligible tempering effect here. The peak temperatures recorded for these locations (Appendix B) did not exceed 771°F(410°C). The time-temperature data indicated that the time spent at these temperatures was on the order of only a few seconds, so no appreciable tempering was expected.

2. Thermocouple Locations 1-3, 3-3

Thermocouples 1-3 and 3-3 were located at distances of 7.25 millimeters (0.29 inch) and 8.4 millimeters (0.33 inch) respectively from the fusion line after welding. The micrographs shown in Figures 26 and 27 again are similar to each other and are not very different from those at thermocouple

locations 1-4 and 3-4 discussed previously. The microstructure is again that of tempered martensite, indicative of the base metal structure. As these thermocouples were also located outside of the HAZ, no significant change in microstructure was expected. The banding which appears in the micrographs is due to segregation in the original ingot which is aligned in the rolling direction upon rolling the ingot into plate. The carbon extraction replicas still indicate the presence of both coarse and fine carbides normally found in tempered martensitic structures. The microhardness measurements made at the thermocouple locations (Table VI) again concur with the Rockwell hardness measurements made on the base metal. Thermocouple 1-3 recorded a peak temperature of 1062°F (572°C) which could have produced some very slight amount of additional tempering.

3. Thermocouple Locations 3-2, 1-2, 2-2

Thermocouple 3-2 was located close to the HAZ, but approximately 1 millimeter (0.04 inches) outside it. The microstructure at this location is presented in Figure 28 and consists of tempered martensite resembling that of the base metal structure. The structure is however, more typical of that found in the dark etching bands of the plate. The carbon extraction replica made at this location is also comparable to that obtained for thermocouples located in the base metal, outside the HAZ. The microhardness measurements made at the point of attachment of the thermocouple indicated

a higher hardness than that of the base metal with a value of 334 on the Vickers scale. This higher hardness does not correlate well with the microstructural evidence presented. The actual hardness measurements made varied from a low of 317 to a high of 358 on the Vickers scale, with an average of 334. The wide variation in values (and the resultant high average value) may be due to the variation in the dispersion of coarse and fine carbides present. The peak temperature recorded by thermocouple 3-2 was 893°F (478°C) which was below the A_1 temperature. This would confirm that the thermocouple was located outside the HAZ as it was not heated into the inter-critical region. No significant change in the microstructure from that of the tempered martensite base metal would be expected, and none was found.

Thermocouple 1-2 was located 3.9 millimeters (0.15 inches) from the fusion line after welding, just inside the fine grained region of the HAZ. Thermocouple 2-2 was located 4.2 millimeters (0.16 inches) from the fusion line after welding, at the edge of the fine grained region of the HAZ. However, the fusion line is not parallel to the bottom of the thermocouple hole for location 2-2 and at one point is only 3 millimeters (0.12 inches) away from it. It is likely, then, that a temperature gradient existed along the bottom of the thermocouple hole, and this would help explain why the peak temperature recorded at this location (1250°F, 677°C) was much lower than that recorded by the similar location 1-2 (1424°F, 773°C). The

microstructure at locations 1-2 and 2-2 is presented in Figures 29 and 30 respectively. Both locations exhibited a very fine martensitic structure typical of the fine grained portion of the HAZ.

In the carbon extraction replicas made at these locations, some carbides appear to remain undissolved by the thermal cycle. The fine carbides present in the base metal, as shown in Figures 24 through 27, have dissolved, but the coarser carbides remain. At location 1-2, fewer of the coarse carbides remain than at location 2-2. This is probably a result of the double austenitizing treatment at location 1-2 caused by the first two weld passes there. The microhardness data shown in Table VI also indicates that more carbon has been dissolved at location 1-2 as a higher hardness exists there than at location 2-2. Both of these locations exhibit a hardness much higher than that of the base metal, and their hardness is consistent with the microhardness traverses.

4. Thermocouple Locations 1-1, 2-1, 4-1

Thermocouple 1-1 was located at the fusion line after welding. The thermal history recorded for this location is not considered accurate as the recording equipment used operated intermittently during the first seven weld passes. The thermal history has been reconstructed as carefully as possible and is included for information purposes only. The micrographs presented in Figure 31 are included as an example of the microstructure at the fusion line where some mixing of

the weld metal and base metal has taken place. The microstructure is that of coarse martensite. The carbon extraction replica at this location has revealed the detail of the martensite and fine carbides can be seen to have formed preferentially along the martensite laths. It is believed that these carbides have formed as a result of the tempering effect of subsequent weld passes.

Thermocouples 2-1 and 4-1 were located very near the fusion line at distances of 1.0 millimeters (0.04 inches) and 0.4 millimeters (0.016 inches) from it respectively. The microstructure at thermocouple location 2-1 is shown in Figure 32, and consists of coarse martensite with some fine carbides formed preferentially along the martensite laths. The peak temperature recorded by this thermocouple was 2301°F (1260°C) indicating that this region had been completely re-austenitized by the nearest weld pass (pass number 12). It was subjected to some tempering by the final three weld passes, which produced the carbides shown in the carbon extraction replica. The microhardness measurements made at the point of attachment of thermocouple 2-1 (Table VI) indicate a hardness value of 335 on the Vickers scale which compares favorably to the fusion line hardness measured during the microhardness traverses performed on the temper bead sequence and with the Rockwell hardness measurements made there. The carbides shown in the carbon extraction replica are smaller than those found in the base metal, though of the same shape and approximate distribution

indicating that this region was not as heavily tempered as the base metal. The microhardness measurements confirm this observation.

Thermocouple 4-1 was mounted at the location of the last pass on the straight sequence welded side of the test plate, and was 0.4 millimeters (0.016 inch) from the fusion line after welding. The microstructure of the metal at this thermocouple location is shown in Figure 33, and consists entirely of untempered martensite. Since this was the location of the last pass, no evidence of tempering was expected and none was found. The dark spherical spot appearing in the 1400X micrograph is not an inclusion or void but is the remnant of a small depression created in the bottom of the thermocouple hole during drilling. The carbon extraction replica indicates the relief in the surface of the sample produced during etching, but shows no evidence of the presence of carbides. The peak temperature recorded by thermocouple 4-1 was 2242°F (1228°C), but it is felt that this value is erroneously low. Since this thermocouple was located closer to the fusion line than thermocouple 2-1, the peak temperature experienced here would be expected to be higher. A possible reason for the lower peak temperature is suggested by Figure 12. The bottom of the thermocouple hole may have retreated away from the fusion line area (buckled upwards into the thermocouple hole) with the approach of the weld bead, effectively moving the thermocouple away from the weld bead. A gap between the bottom of

the weld bead and the bottom of the thermocouple hole is evident in Figure 12, and the hole bottom has taken on a concave appearance. The microhardness measurements made at the thermocouple attachment point (Table VI) indicate a hardness value of 382 on the Vickers scale. This value agrees with both the Rockwell hardness measurement made at the fusion line and with the data obtained from the microhardness traverse performed at the last pass of the straight bead sequence. The high hardness, equivalent to approximately 38 R_C , is also in agreement with the microstructural evidence which indicated that none of the carbon had precipitated as carbides. The high hardness would be expected in an area that was untempered, as was the case here.

F. ADDITIONAL OBSERVATIONS

The plot of the peak temperature versus distance from the fusion line (Fig. 19), when combined with the average width of the visible HAZ (3.95 mm), suggests that the A_1 temperature is elevated by rapid heating to approximately 1350°F (732°C).

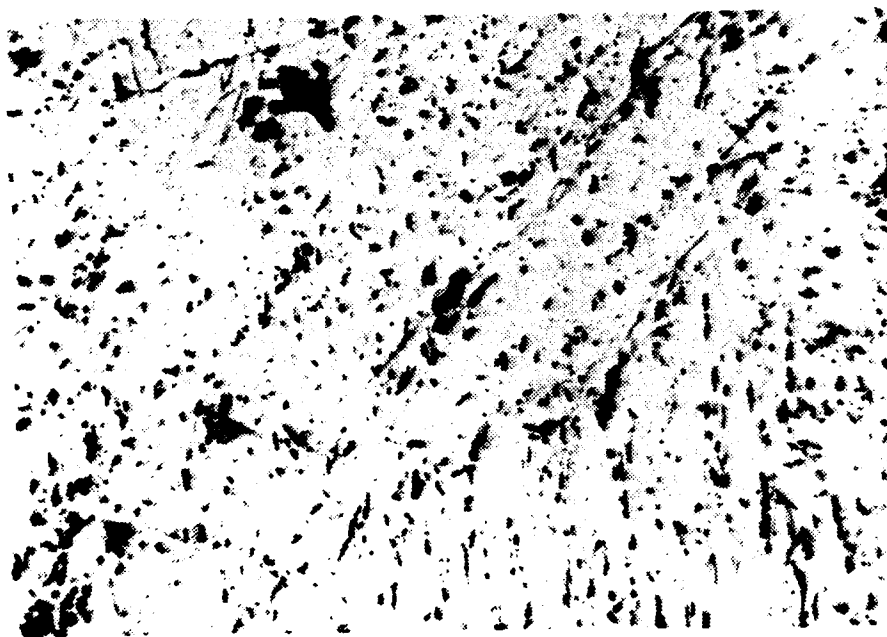
The microhardness traverses conducted coupled with the microstructural analysis indicates that significant tempering in the HAZ can be caused by subsequent weld passes. The tempering lowers the overall hardness of the HAZ and may increase the distance over which the hardness decreases from that of the HAZ to that of the base metal. This is probably due to a more rapid tempering response of the metal at the



560X 5% Nital



1400X 5% Nital



8000X

TEM

Carbon Extraction Replica

Figure 24. Location 1-4, 12.2 mm from the fusion line after welding.



560X 5% Nital



1400X 5% Nital



8000X TEM Carbon Extraction Replica

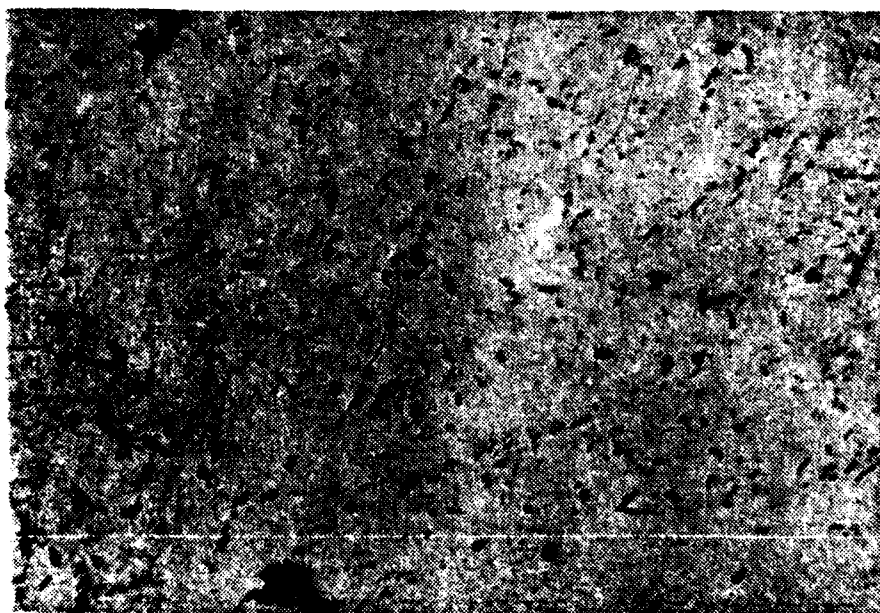
Figure 25. Location 3-4, 12.4 mm from the fusion line after welding.



560X 5% Nital



1400X 5% Nital



3000X TEM Carbon Extraction Replica

Figure 26. Location 1-3, 7.25 mm from the fusion line after welding.



560X 5% Nital

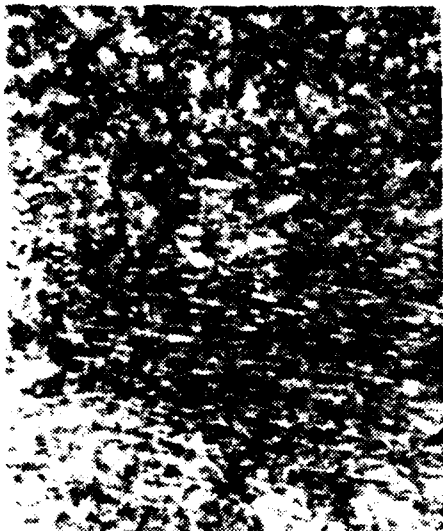


1400X 5% Nital



8000X TEM Carbon Extraction Replica

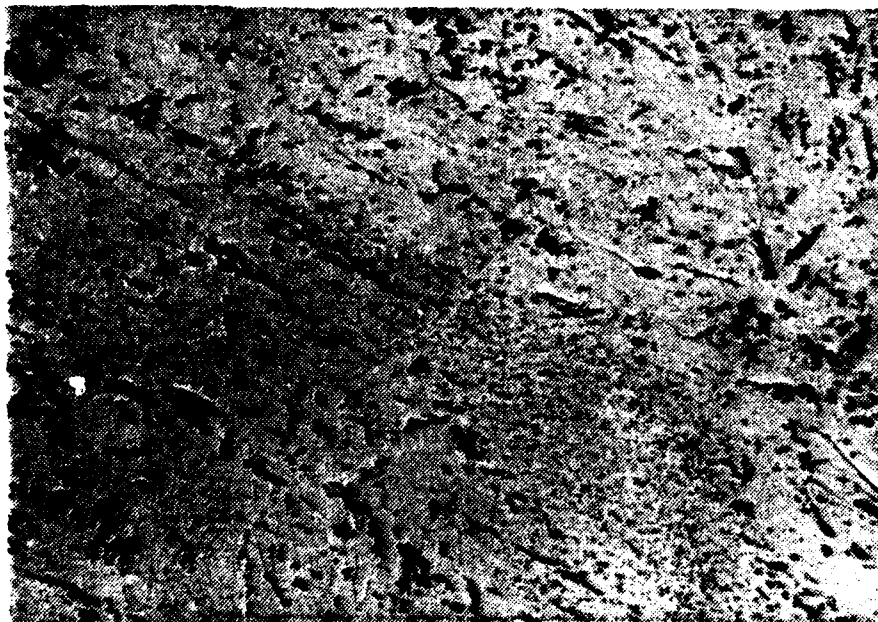
Figure 27. Location 3-3, 8.4 mm from the fusion line after welding.



560X 5% Nitai

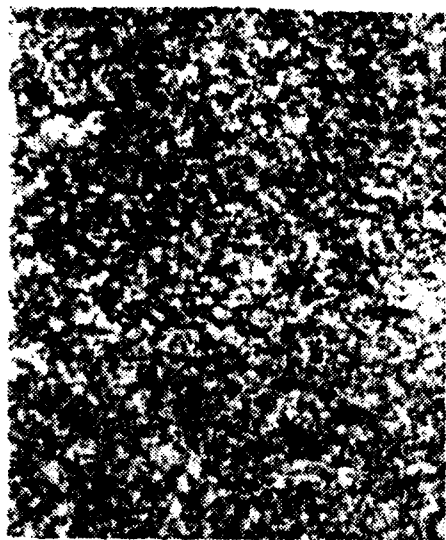


1400X 5% Nitai

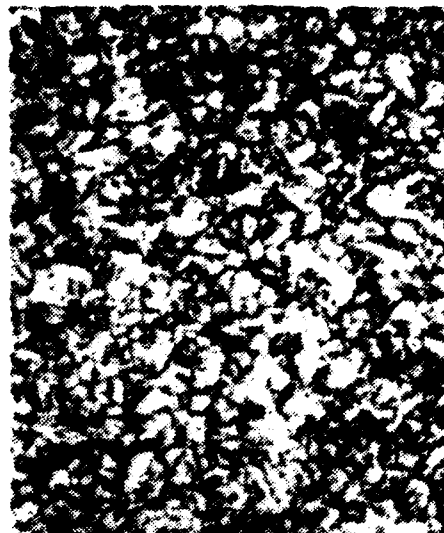


8000X TEM Carbon Extraction Replica

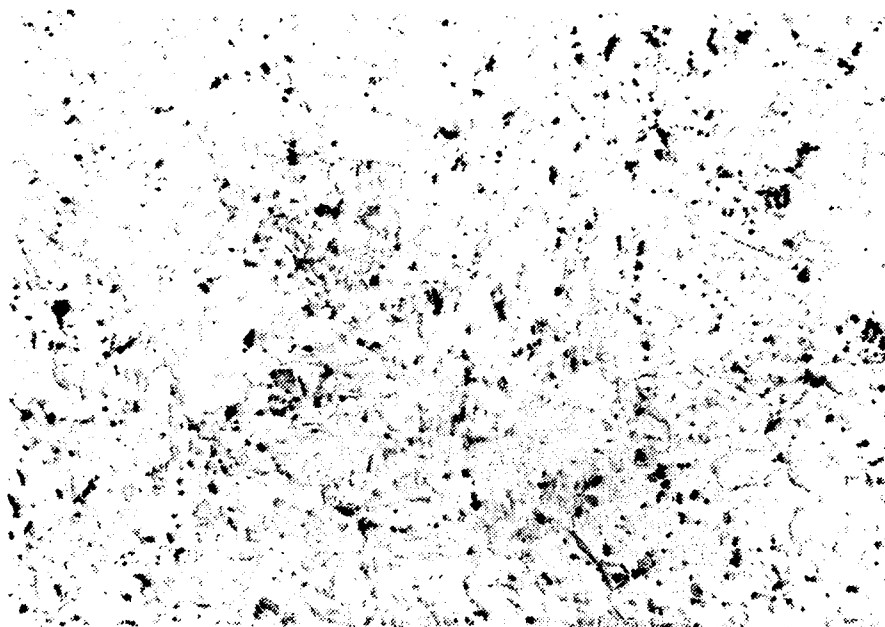
Figure 28. Location 3-2, 5.6 mm from the fusion line after welding.



560X 5% Nital

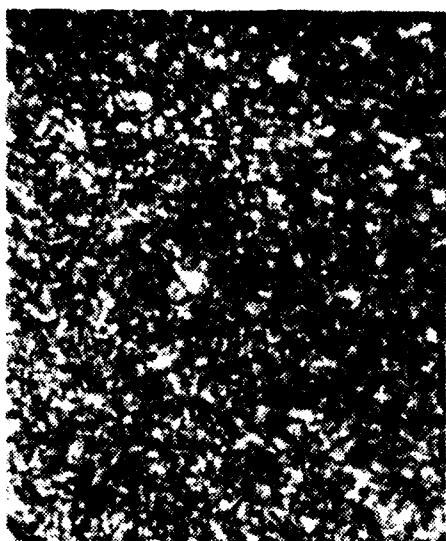


1400X 5% Nital



8000X TEM Carbon Extraction Replica

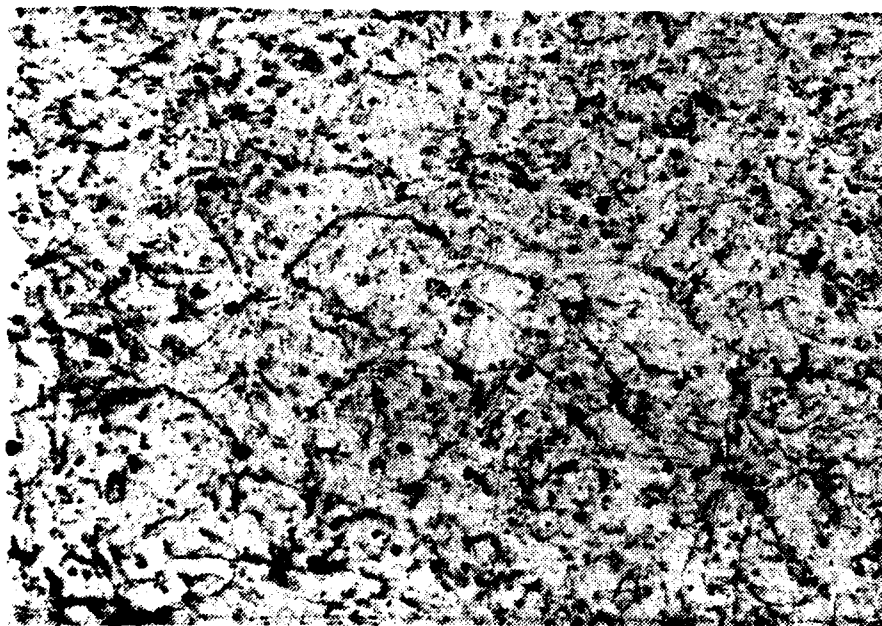
Figure 29. Location 1-2, 3.9 mm from the fusion line after welding.



560X 5% Nital



1400X 5% Nital

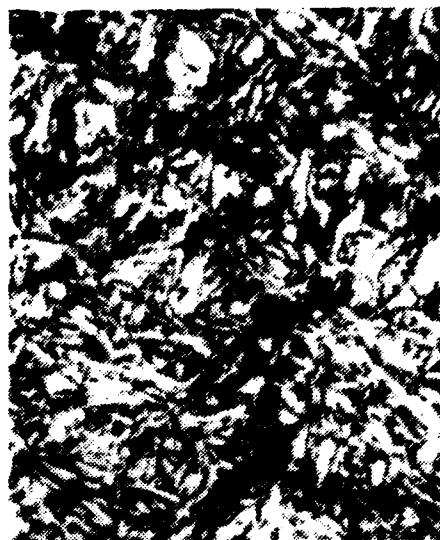


8000X TEM Carbon Extraction Replica

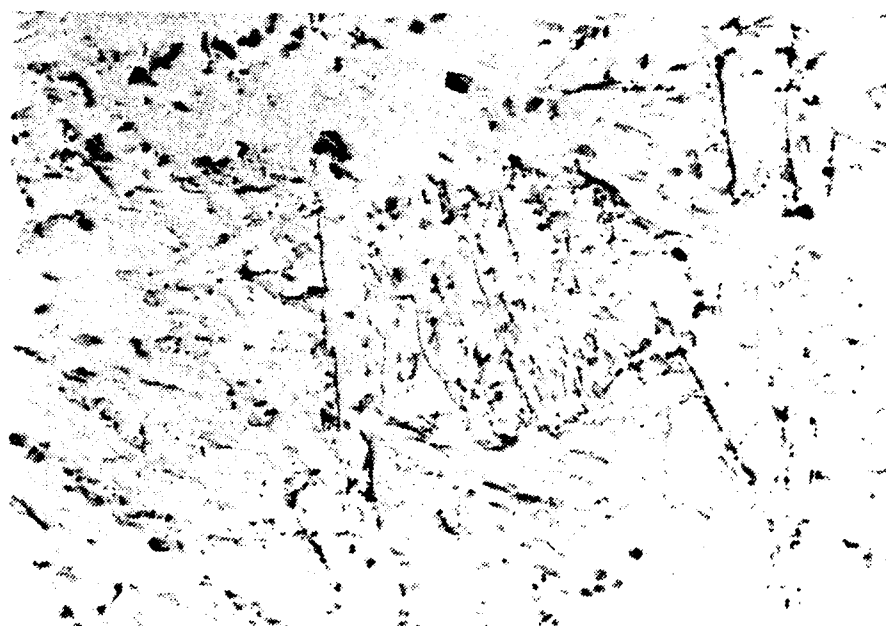
Figure 30. Location 2-2, 4.2 mm from the fusion line after welding.



560X 5% Nitral



1400X 5% Nitral



8000X TEM Carbon Extraction Replica

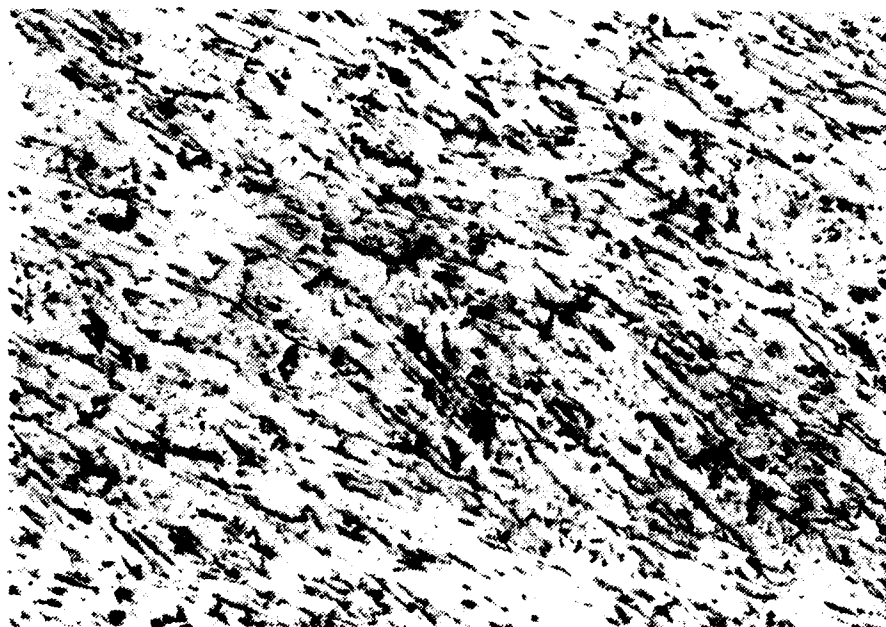
Figure 31. Location 1-1, at the fusion line after welding.



560X 5% Nital



1400X 5% Nital



3000X TEM Carbon Extraction Replica

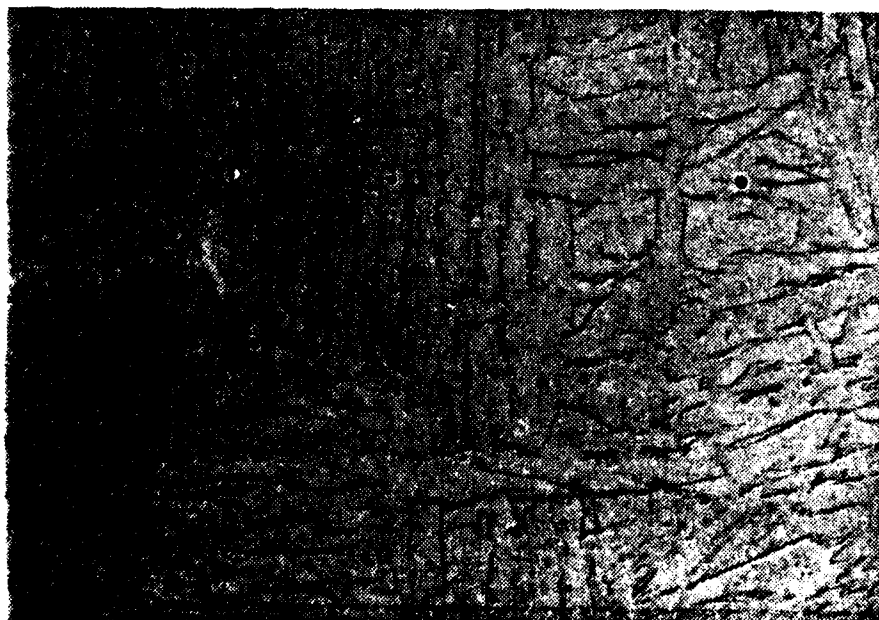
Figure 32. Location 2-1, 1.0 mm from the fusion line after welding.



560X 5% Nital



1400X 5% Nital



3000X TEM Carbon Extraction Replica

Figure 33. Location 4-1, 0.1 mm from the fusion line after welding.

edge of the visible HAZ. In support of this explanation, the following argument is offered:

Austenite formed by heating the steel into the relatively low temperature intercritical region will have a higher carbon content than the bulk composition. Thus, the martensite which is formed from it on rapid cooling should have a higher hardness than that formed from fully austenitized steel. Only a fraction of the microstructure, however, will be martensite. The remainder will be composed of a mixture of ferrite and carbides. High carbon martensites are known to temper more quickly than low carbon martensites [Ref. 22]. Therefore, for a given amount of tempering, the hardness of the material heated nearest the A_1 temperature should decrease more than that of material heated to higher temperatures.

This effect appears to have occurred only at locations very near the edge of the visible HAZ, as is demonstrated by comparing the results of the microhardness traverse shown in Figure 20 with that shown in Figure 22. Evidence in support of the above stated argument is obtained by combining the information presented in Figures 19 and 20. In doing so, it is found that the hardness of the HAZ, at the locations where the steel was heated into the intercritical region, is slightly higher than at locations which were heated to above the A_3 temperature.

The low hardness observed at the fusion line is a surprising result as Brucker [Ref. 23] did not report this observation. His microhardness measurements conducted on cast HY-130 plates, were performed at 0.25 millimeter (0.01 inch) intervals in the vicinity of the fusion line. As a result, the minimum hardness occurring at the fusion line could have easily been missed. Re-examination of his data on the cast HY-130 plates

has revealed a minimum hardness at the fusion line in all hardness traverses that he performed. Neither the optical microscopy performed in the course of this research, nor that performed by Brucker provides any indication as to why this minimum exists. One possible explanation is the formation of the delta ferrite phase (with its attendant very low carbon solubility) in the vicinity of the fusion line. Thin foil transmission electron microscopy may provide a clue as to the cause of the low hardness at the fusion line.

IV. CONCLUSIONS

Based on the research conducted and the results obtained, the following conclusions are drawn:

1. A severe hardness gradient (and corresponding strength gradient) does exist near the edge of the heat affected zone at the location of the last weld pass in a HY-130 plate welded with the straight bead sequence technique, supporting the "metallurgical notch" theory postulated by Brucker.
2. Subsequent weld passes do produce some tempering effects in the initial weld passes and their associated heat affected zones.
3. A definite relationship exists between the thermal history during welding, the hardness and the microstructure observed.
4. The fusion line hardness is significantly lower than that of adjacent weld and base metal.
5. No significant changes in the microstructure of the welded plate occur outside of the heat affected zone.
6. The technique used during welding (i.e. temper bead, straight sequence, etc.) does make a definite difference in the properties of the base metal's heat affected zone.

V. RECOMMENDATIONS

Based on the research conducted, the results obtained and the conclusions drawn, the following recommendations are offered:

1. An in-depth, quantitative as well as qualitative study of the tempering effects in the heat affected zone be undertaken, possibly through the use of Transmission Electron Microscopy.
2. A comparison of the thermal history data obtained from the instrumented weld be made with thermal histories predicted by existing computer programs and the programs updated as necessary.
3. Macroscopic sized samples of the heat affected zone be produced in the laboratory and tested mechanically to determine strength, fracture toughness and crack initiation and propagation properties.
4. As an interim measure, pending completion of the recommended studies, all future welds in thick sections of HY-130 steel be made using the temper bead technique.

APPENDIX A

<p>MARE ISLAND NAVAL SHIPYARD</p> <p>WELDING PROCEDURE QUALIFICATION RECORD</p>		<p>Lab. Test No. 32-80-1</p> <p>Welding Proc. No. H-11-3 RAYB</p> <p>Page 1 of 3</p> <p>Date 11-17-80</p>
<p>Material HY-130 Specification MIL-S-24371A to HY-130 MIL-S-24371A</p>		<p>D or S No. To</p>
<p>Material Condition PAINTED</p>	<p>Base Mat'l Cleaning DISC SAND</p>	
<p>Material Type or Classification HY-130</p>	<p>Method of Edge Prep. PLANE BEVEL</p>	
<p>Thickness 1 15/16</p>	<p>If Mat'l is Pipe, Dia. and Wall Thickness</p>	
<p>Thickness Range This Test Qualified</p>		
<p>Filler Material Specification & Type MIL-E-24355A MIL-1405-1 HEAT #51252 1/16" 6</p>		
<p>Describe Filler Material if not Described in Applicable Specification NOTE: PLY PREP JO 3 91-28033000-000</p>		
<p>PLY PROVIDED HY-130 PROGRAM NM-101-78</p>		
<p>Flux Composition Specification Size, Type NA</p>	<p>Postweld Heat Treatment</p>	
<p>Backing Ring or Strip Mat'l, Type NA</p>	<p>Consumable Insert Type, Size, Spec. NA</p>	
<p>SPEC. JOINT DESIGN NO.</p>	<p>BEAD PATTERN</p>	
	<p>B SIDE 1</p> <p>A SIDE 1</p> <p>LKG OPPOSITE DIRECTION OF TRAVEL.</p> <p>B SIDE 2</p> <p>A SIDE 2</p>	
<p>WELD PROGRESS/DEPOSITION SEQUENCE</p>	<p>TORCH, WIREFEED RELATIONSHIP AND LOCATION</p>	
<p>NOTE: SIDE 1 USE TEMPER BEAD SIDE 2 NO TEMPER BEAD. ESTABLISH SIDE 1 PARAMETERS TO DUPLICATE PLATE #6 ESCO & SIDE 2 TO DUPLICATE PLATE #</p>		

MARE ISLAND NAVAL SHIPYARD
WELDING PROCEDURE QUALIFICATION RECORD

WELDING NO.

32-80-1

Welding

Proc. No.

Page 2 of 3

WELDING DATA SIDE 1

WELD ALL PRIOR TO
TURNING

		1	2	3	4	5
GENERAL	Spec. No.					
	Process	GMA SPRAY				
	Man. Spec. No.	AUT 2				
EQUIPMENT	Welding Position	FLAT				
	Power Source (Manual or Auto)					
	Auto Voltage Control					
ELECTRODE	Type					
	Size (Inch)					
	Tip Contamination					
FILLER METAL	Welding Metal	MIL-1405				
	Size (Inch)	1/16" Ø				
	Shielding Gas	98/2 2.0/1				
WELDING	Gas Flow Rate (SCFH)	40 - 45				
	Cup/Nozzle (Inch)					
	Electrode Extension (Inch)					
PURGING	Back Purge (SCFH)	5/8	3/4	3/4	3/4	3/4
	Gas Flow Rate (SCFH)					
	Preheat/Interpass Temp (°F)	200°F				
PREHEAT/INTERPASS	Interpass Temp (°F)	TEMP. STK				
	Interpass Time (Sec)	50				
	Method of Measuring Temperature	TEMP. STK PYROMETER CTR 14-0395-00				
ELECTRICAL CHARACTER	Current (Amps) or Voltage (Volts)	DC RD				
	Slope					
	Pulse Frequency (Hz)					
WELDING PARAMETERS	Pulse Peak (Volts)					
	Pulse Width (Sec)					
	Peak - Background - Ratio					
WELDING PARAMETERS	Arc Initiation, Number of					
	Amps	400	425	400	400	400
	Volts	27	27	27	27	27
WELDING PARAMETERS	Wire Feed Speed (Inch/Min)					
	Travel Speed (Inch/Min)	12.5	12.5	12.5	12.5	12.5
	Arc Decay (Sec)					
AUTOMATIC WELDING	Gas Flow Rate (SCFH)					
	Wire Feed Speed (Inch/Min)					
	Gas Flow Rate (SCFH)					
OTHER SPECIFY	Heat Input (KJ/Inch)	5.2				
* AUG 26-80 DUE AUG. 26-81						

Only 1: other than electrode.

MADE ISLAND NAVAL SHIPYARD
WELDING PROCEDURE QUALIFICATION RECORD

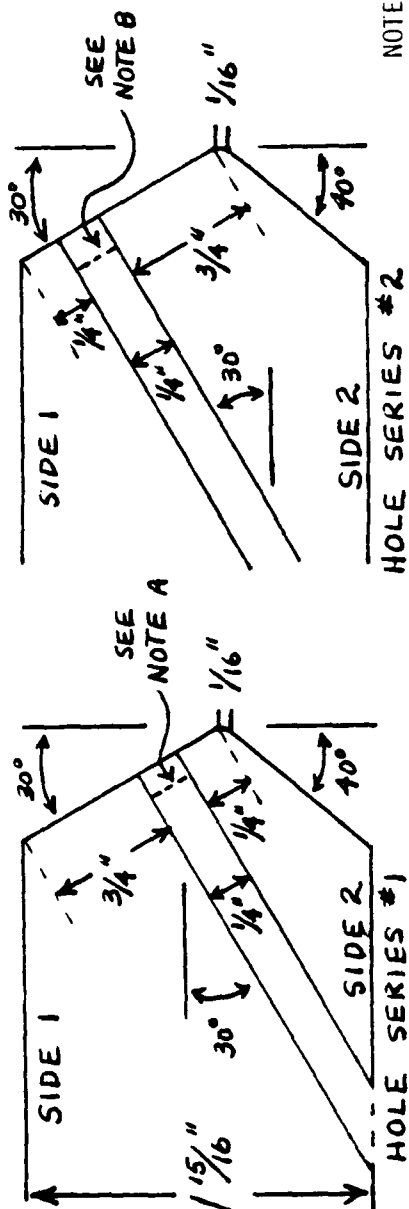
Welding
Proc. No.

Page 3 of 3

WELDING DATA SIDE 1 WELD ALL PRIOR TO TURNING

GENERAL	Base No.	6-27
	Process	
EQUIPMENT	Man. Spec. Assn. Date	
	Welding Position	
	Welding Machine	
	Auto Voltage Control	
ELECTRODE	Type	
	Size (mm)	
	Tig Configuration	
	Method of Preparation	
FILLER METAL*	Size (mm)	
WELDING	Gas Flow Rate (ccm)	
	Cup/Nozzle Position (mm)	
	Electrode Position (mm)	
	Nozzle to Work Distance (mm)	
	Contact to Work Distance (mm) 2/4	
PURGING	Gas Flow Rate (ccm)	
	Gas Flow Rate (ccm)	
PREHEAT/INTERPASS	Preheat Temperature (°F)	
	Interpass Temperature (°F)	250
	Method of Measuring Preheat	
ELECTRICAL CHARACTER	Current Type and Polarity	
	Open Circuit Voltage	
	Stroke	
	Pulse Frequency (Hz)	
	Pulse Peak (Vrms/Volts)	
	Pulse Duty Cycle (Hz/Volts)	
	Peak - Background - Time Ratio	
	Arc Initiation, Method of	
WELDING PARAMETERS	Amperes	400
	Volts	27
	Wire Feed Rate (mm)	
	Travel Speed (mm)	12.5
	Arc Decay (sec)	
AUTOMATIC WELDING	Osc. Frequency (Hz)	
	Osc. Width (mm)	
	Osc. Depth (mm)	
OTHER SPECIFY	Heat Input (kJ/in)	

*Only if other than electrode.



NOTE A

HOLE SERIES #2

SIDE VIEWS

DISTANCE
FROM BEVEL

HOLE #

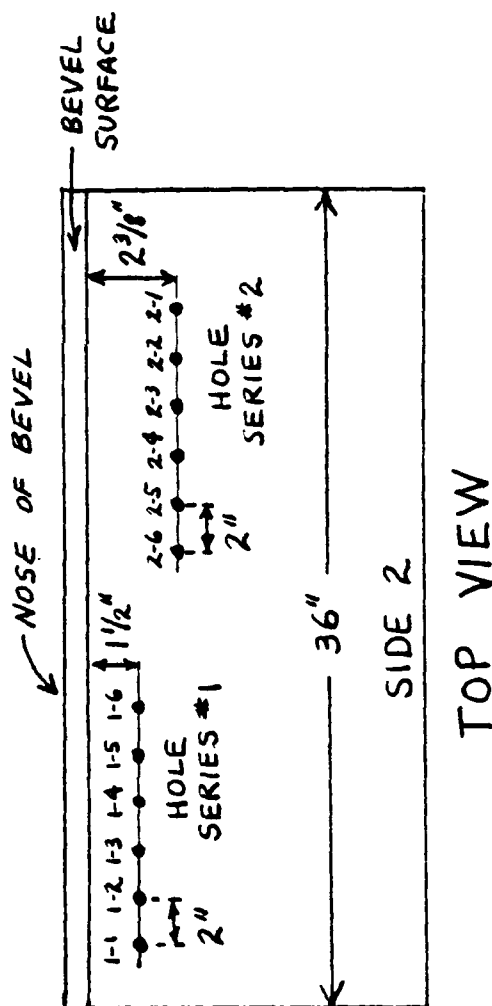
1-1	.08"
1-2	.20"
1-3	.35"
1-4	.50"
1-5	.70"
1-6	1.00"

NOTE B

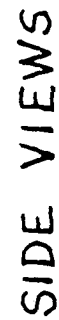
DISTANCE
FROM BEVEL

HOLE #

2-1	.08"
2-2	.20"
2-3	.35"
2-4	.50"
2-5	.70"
2-6	1.00"



TOP VIEW



HOLE #	DISTANCE FROM BEVEL
1	1.0
2	1.0
3	1.0
4	1.0
5	1.0
6	1.0
7	1.0
8	1.0
9	1.0
10	1.0
11	1.0
12	1.0
13	1.0
14	1.0
15	1.0
16	1.0
17	1.0
18	1.0
19	1.0
20	1.0
21	1.0
22	1.0
23	1.0
24	1.0
25	1.0
26	1.0
27	1.0
28	1.0
29	1.0
30	1.0
31	1.0
32	1.0
33	1.0
34	1.0
35	1.0
36	1.0
37	1.0
38	1.0
39	1.0
40	1.0
41	1.0
42	1.0
43	1.0
44	1.0
45	1.0
46	1.0
47	1.0
48	1.0
49	1.0
50	1.0
51	1.0
52	1.0
53	1.0
54	1.0
55	1.0
56	1.0
57	1.0
58	1.0
59	1.0
60	1.0
61	1.0
62	1.0
63	1.0
64	1.0
65	1.0
66	1.0
67	1.0
68	1.0
69	1.0
70	1.0
71	1.0
72	1.0
73	1.0
74	1.0
75	1.0
76	1.0
77	1.0
78	1.0
79	1.0
80	1.0
81	1.0
82	1.0
83	1.0
84	1.0
85	1.0
86	1.0
87	1.0
88	1.0
89	1.0
90	1.0
91	1.0
92	1.0
93	1.0
94	1.0
95	1.0
96	1.0
97	1.0
98	1.0
99	1.0
100	1.0

HOLE #	DISTANCE FROM BEVEL
1	1.0
2	1.0
3	1.0
4	1.0
5	1.0
6	1.0
7	1.0
8	1.0
9	1.0
10	1.0
11	1.0
12	1.0
13	1.0
14	1.0
15	1.0
16	1.0
17	1.0
18	1.0
19	1.0
20	1.0
21	1.0
22	1.0
23	1.0
24	1.0
25	1.0
26	1.0
27	1.0
28	1.0
29	1.0
30	1.0
31	1.0
32	1.0
33	1.0
34	1.0
35	1.0
36	1.0
37	1.0
38	1.0
39	1.0
40	1.0
41	1.0
42	1.0
43	1.0
44	1.0
45	1.0
46	1.0
47	1.0
48	1.0
49	1.0
50	1.0
51	1.0
52	1.0
53	1.0
54	1.0
55	1.0
56	1.0
57	1.0
58	1.0
59	1.0
60	1.0
61	1.0
62	1.0
63	1.0
64	1.0
65	1.0
66	1.0
67	1.0
68	1.0
69	1.0
70	1.0
71	1.0
72	1.0
73	1.0
74	1.0
75	1.0
76	1.0
77	1.0
78	1.0
79	1.0
80	1.0
81	1.0
82	1.0
83	1.0
84	1.0
85	1.0
86	1.0
87	1.0
88	1.0
89	1.0
90	1.0
91	1.0
92	1.0
93	1.0
94	1.0
95	1.0
96	1.0
97	1.0
98	1.0
99	1.0
100	1.0



APPENDIX B

THERMAL HISTORY DATA OBTAINED FROM TIME-TEMPERATURE PLOTS

THERMOCOUPLE #1-1

SIDE #1

CHANNEL #1

WELD SEQUENCE TEMPER BEAD

BASE TEMPERATURE (AVERAGE) 280°F					
PASS #	PEAK (°F) TEMPERATURE	TIME FROM BASE TEMP TO PEAK			TIME FROM PEAK TO BASE TEMP
1	1518 *	8.4	Sec	*	14.2 Min
2	1500 *	8.4	"	*	UNREADABLE "
3	595 *	16.8	"	*	15.2 "
4	1162 *	9.6	"	*	10.0 "
5	493 *	20.4	"	*	9.6 "
6	756 *	13.2	"	*	7.0 "
7	569 *	18.0	"	*	12.2 "
8	426	28.8	"		6.8 "
9	616	15.6	"		14.7 "
10	509	22.8	"		24.1 "
11	390	52.8	"		16.4 "
12	504	24.0	"		19.4 "
13	453	40.8	"		17.4 "
14	495	30.0	"		16.7 "
15	477	40.8	"		13.3 "

*Note Channel Intermittent for first 7 weld passes.

THERMOCOUPLE #1-2

SIDE #1

CHANNEL #2

WELD SEQUENCE TEMPER BEAD

BASE TEMPERATURE (AVERAGE) 250°F				
PASS #	PEAK (°F) TEMPERATURE	TIME FROM BASE TEMP TO PEAK		TIME FROM PEAK TO BASE TEMP
1	1600	9.6	Sec	20.7 Min
2	1424	10.8	"	UNREADABLE "
3	718	13.2	"	16.6 "
4	1068	7.2	"	16.9 "
5	573	18.0	"	13.6 "
6	767	14.4	"	14.4 "
7	591	18.0	"	11.5 "
8	426	27.6	"	7.0 "
9	608 *	15.6 ***		14.0 ** "
10	530	21.6	"	23.1 "
11	399	45.6	"	15.8 "
12	500	28.8	"	19.3 "
13	453	38.4	"	17.8 "
14	484	33.6	"	16.5 "
15	473	34.8	"	18.2 "

*Questionable reading peak erratic.

**Estimated Reading

THERMOCOUPLE #1-3

SIDE #1

CHANNEL #3

WELD SEQUENCE TEMPER BEAD

BASE TEMPERATURE (AVERAGE) 250°F					
PASS #	PEAK (°F) TEMPERATURE	TIME FROM BASE TEMP TO PEAK		TIME FROM PEAK TO BASE TEMP	
1	1062	4.8	Sec	25.2	Min
2	727	14.4	"	20.6	"
3	443	34.8	"	17.9	"
4	577	15.6	"	18.9	"
5	409	43.2	"	13.9	"
6	520	20.4	"	17.4	"
7	432	56.4	"	15.3	"
8	319	75.6	"	4.9	"
9	477	48.0	"	11.1	"
10	405	67.2	"	17.1	"
11	301	120.0	"	7.4	"
12	452	72.0	"	12.2	"
13	375	86.4	"	10.3	"
14	418	75.6	"	8.2	"
15	366	85.2	"	8.2	"

THERMOCOUPLE #1-4

SIDE #1

CHANNEL #4

WELD SEQUENCE TEMPER BEAD

BASE TEMPERATURE (AVERAGE) 360°F				
PASS #	PEAK (°F) TEMPERATURE	TIME FROM BASE TEMP TO PEAK		TIME FROM PEAK TO BASE TEMP
1	771	13.2	Sec	UNREADABLE Min
2	739	14.4	"	UNREADABLE "
3	558	20.4	"	14.8 "
4	692	16.8	"	15.3 "
5	509	28.8	"	13.3 "
6	627	18.0	"	16.5 "
7	537	30.0	"	10.0 "
8	441	48.0	"	3.6 "
9	586	24.0	"	11.9 "
10	522	37.2	"	19.3 "
11	455	66.0	"	13.9 "
12	563	33.6	"	18.6 "
13	496	58.8	"	16.4 "
14	543	44.8	"	15.4 "
15	519	48.0	"	11.0 "

THERMOCOUPLE #2-1

SIDE #1

CHANNEL #12

WELD SEQUENCE TEMPER BEAD

BASE TEMPERATURE (AVERAGE) 250°F					
PASS #	PEAK (°F) TEMPERATURE	TIME FROM BASE TEMP TO PEAK		TIME FROM PEAK TO BASE TEMP	
1	453	30.0	Sec	12.2	Min
2	575	20.4	"	UNREADABLE "	
3	385	30.0	"	12.7	"
4	1015	7.2	"	12.6	"
5	372	24.0	"	9.6	"
6	1463	9.6	"	11.4	"
7	583	19.2	"	8.8	"
8	354	26.4	"	5.9	"
9	1596	10.8	"	11.2	"
10	624	14.4	"	15.6	"
11	347	57.6	"	10.8	"
12	2301	2.4	"	16.6	"
13	455	26.4	"	14.9	"
14	1011	15.6	"	14.4	"
15	656	19.2	"	16.5	* "

*Estimated

THERMOCOUPLE #2-2

SIDE #1

CHANNEL #11

WELD SEQUENCE TEMPER BEAD

BASE TEMPERATURE (AVERAGE) 260°F				
PASS #	PEAK (°F) TEMPERATURE	TIME FROM BASE TEMP TO PEAK		TIME FROM PEAK TO BASE TEMP
1	502	26.4	Sec	UNREADABLE
2	573	16.8	"	UNREADABLE
3	412	27.6	"	17.0 Min
4	819	10.8	"	13.5 "
5	405	28.8	"	13.4 "
6	953	9.6	"	14.6 "
7	519	20.4	"	UNREADABLE "
8	351	36.0	"	6.6 "
9	1250	8.4	"	17.0 "
10	599	15.6	"	22.8 "
11	376	57.6	"	12.9 "
12	1158	6.0	"	18.7 "
13	450	30.0	"	17.1 "
14	894	12.0	"	15.9 "
15	608	18.0	"	UNREADABLE "

THERMOCOUPLE #3-2

SIDE #2

CHANNEL #2

WELD SEQUENCE STRAIGHT BEAD

BASE TEMPERATURE (AVERAGE) 250°F					
PASS #	PEAK (°F) TEMPERATURE	TIME FROM BASE TEMP TO PEAK		TIME FROM PEAK TO BASE TEMP	
1	778	12.0	Sec	23.4	Min
2	893	10.8	"	21.4	"
3	506	20.4	"	17.26	"
4	665	14.4	"	17.5	"
5	435	25.2	"	21.2	"
6	793	12.0	"	29.8	"
7	600	18.0	"	20.64	"
8	392	42.0	"	15.8	"
9	437	27.6	"	13.0	"
10	545	21.6	"	12.3	"
11	622	18.0	"	13.7	"

THERMOCOUPLE #3-3

SIDE #2

CHANNEL #3

WELD SEQUENCE STRAIGHT BEAD

BASE TEMPERATURE (AVERAGE) 270°F				
PASS #	PEAK (°F) TEMPERATURE	TIME FROM BASE TEMP TO PEAK		TIME FROM PEAK TO BASE TEMP
1	707	13.2	Sec	24.3 Min
2	833	10.8	"	21.2 "
3	500	16.8	"	17.1 "
4	641	14.4	"	18.0 "
5	435	25.2	"	UNREADABLE "
6	737	12.0	"	33.0 "
7	571	14.4	"	25.6 "
8	403	40.8	"	25.0 "
9	435	28.8	"	21.2 "
10	536	21.6	"	14.7 "
11	603	15.6	"	20.2 "

THERMOCOUPLE #3-4

SIDE #2

CHANNEL #4

WELD SEQUENCE STRAIGHT BEAD

BASE TEMPERATURE (AVERAGE) 270°F				
PASS #	PEAK (°F) TEMPERATURE	TIME FROM BASE TEMP TO PEAK		TIME FROM PEAK TO BASE TEMP
1	610	13.2	Sec	23.9 Min
2	696	14.4	"	21.6 "
3	466	24.0	"	17.4 "
4	560	20.4	"	17.6 "
5	412	33.6	"	UNREADABLE "
6	612	14.4	"	34.4 "
7	502	21.6	"	25.5 "
8	385	48.0	"	24.2 "
9	403	36.0	"	19.4 "
10	461	25.2	"	14.6 "
11	519	21.6	"	19.3 "

THERMOCOUPLE #4-1

SIDE #2

CHANNEL #12

WELD SEQUENCE STRAIGHT BEAD

BASE TEMPERATURE (AVERAGE) 250°F			
PASS #	PEAK (°F) TEMPERATURE	TIME FROM BASE TEMP TO PEAK	TIME FROM PEAK TO BASE TEMP
1	345 *		
2	1235		NOTE:
3	459		Time data unavailable
4	767		as time scale was dis-
5	410		continuous - problems
6	2242 **		with recorder stopping
7	840		between weld passes.
8	UNREADABLE		
9	605		
10	880		
11	1428		

*Estimated

**Readings believed low from this point onward as thermocouple may have moved (see results).

LIST OF REFERENCES

1. Department of Defense Procurement Specification MIL-S-24512, Steel Forgings, Alloy, Structural, High Yield Strength (HY-130), 4 September 1975.
2. Department of Defense Procurement Specification MIL-S-24371 (1), Steel Plate, Structural, High Yield Strength (HY-130), 16 October 1975.
3. Department of Defense Procurement Specification MIL-S-30-C/1, Steel Castings, Alloy, High Yield Strength (HY-130), 27 December 1971.
4. Connor, L. P., Rathbone, A. M. and Gross, J. H., "Development of Procedures for Welding HY-130 (T) Steel," Welding Research Supplement to The Welding Journal, pp 3095-3215, July 1967.
5. Flax, R. W., Keith, R. E. and Randall, M. E., "Welding the HY Steels," American Society for Testing and Materials Special Technical Publication 494, April 1971.
6. Masubuchi, K. and Papazoglou, V. J., "Study of the Residual Stresses and Distortion in Structural Weldments in High-Strength Steels," Second Technical Progress Report, M.I.T. OSP#82558, November 1980.
7. Rogalski, W. J., "An Economic and Technical Study on the Feasibility of Using Advanced Joining Techniques in Constructing Critical Naval Marine Structures," Ocean Engineer Thesis, Massachusetts Institute of Technology, June 1979.
8. Mabry, J. P., "Prediction and Control of Residual Stresses and Distortion in HY-130 Thick Pipe Weldments," Ocean Engineer Thesis, Massachusetts Institute of Technology, May 197.
9. Lipsey, M. D., "Investigation of Welding Thermal Strains in High Strength Quenched and Tempered Steel," Ocean Engineer Thesis, Massachusetts Institute of Technology, June 1978.
10. Brucker, R. B., "Fracture Properties of HY-130 Cast Plate Weldments," Master's Thesis, Naval Postgraduate School, December 1980.

11. Department of the Navy Specification, "Standard Procedures for Preproduction Testing Materials by the Explosion Bulge Test," Revision 1, November 1965.
12. Connor, L. P., Rathbone, A. M. and Gross, J. H., op. cit.
13. Stoop, J. and Metzbowler, E. A., "A Metallurgical Characterization of HY-130 Steel Welds," Welding Research Supplement to The Welding Journal, pp 345S-353S, November 1978.
14. Connor, L. P. and Haak, R. P., "Welding Characteristics of Rapidly Heat-Treated 5Ni-Cr-Mo-V Steel," U.S. Steel Corporation Applied Research Laboratory Report 39.018-002 (32), 1 July 1965.
15. Hollomon, J. H. and Jaffee, L. D., "Time Temperature Relations in Tempering Steel," Transactions, American Institute of Mining and Metallurgical Engineers, Vol. 162, p 223, 1945.
16. Grange, R. A. and Baughman, R. W., "Hardness of Tempered Martensite in Carbon and Low Alloy Steels," Transactions of the American Society for Metals, Vol. 48, p 165, 1956.
17. Zanis, C. A., private communication, 1981.
18. Brucker, R. B., op. cit.
19. Kellock, G. T. B., Sollars, A. R. and Smith, E., "Simulated Weld Heat-Affected Zone Structures and Properties of HY-80 Steel," Journal of the Iron and Steel Institute, p 971, December 1971.
20. Kellock, G. T. B., Sollars, A. R. and Smith, E., ibid., pp 969-974.
21. Cincotta, P. E., "The Effects of Simulated Welds on HY-130 Cast and Wrought Plate and Weld Filler Metal Microstructure," Master's Thesis, Naval Postgraduate School, September 1981.
22. Speich, G. R., "Tempering of Low Carbon Martensite," Transactions of the Metallurgical Society of AIME, Vol. 245, pp 2553-2564, December 1969.
23. Brucker, R. B., op. cit.

INITIAL DISTRIBUTION LIST

	No. Copies
1. Defense Technical Information Center Cameron Station Alexandria, Virginia 22314	2
2. Library, Code 0142 Naval Postgraduate School Monterey, California 93940	2
3. Department Chairman, Code 69 Department of Mechanical Engineering Naval Postgraduate School Monterey, California 93940	1
4. Assistant Professor K. D. Challenger, Code 69Ch Department of Mechanical Engineering Naval Postgraduate School Monterey, California 93940	5
5. Dr. Charles Zanis, Code 2820 David Taylor Research and Development Center Annapolis, Maryland 21402	1
6. Mr. Ivo Fioritti, Code 323 Naval Sea Systems Command National Center, Building 3 2531 Jefferson Davis Highway Arlington, Virginia 20362	1
7. LCDR Michael J. Sorek, USN 98-919C Kaonohi Street Aiea, Hawaii 96701	2
8. Mr. G. Power, Code 138.3 Mare Island Naval Shipyard Vallejo, California 94950	1